Journal of Vertebrate Paleontology

ISSN: (Print) (Online) Journal homepage: https://www.tandfonline.com/loi/ujvp20

Postcranial osteology of the basally branching hadrosauroid dinosaur *Tanius sinensis* from the Upper Cretaceous Wangshi Group of Shandong, China

Niclas H. Borinder, Stephen F. Poropat, Nicolás E. Campione, Tomas Wigren & Benjamin P. Kear

To cite this article: Niclas H. Borinder, Stephen F. Poropat, Nicolás E. Campione, Tomas Wigren & Benjamin P. Kear (2021): Postcranial osteology of the basally branching hadrosauroid dinosaur *Tanius sinensis* from the Upper Cretaceous Wangshi Group of Shandong, China, Journal of Vertebrate Paleontology, DOI: 10.1080/02724634.2021.1914642

To link to this article: https://doi.org/10.1080/02724634.2021.1914642

Journal of Vertebrate Paleontology e1914642 (20 pages)
Published with license by the Society of Vertebrate Paleontology
DOI: 10.1080/02724634.2021.1914642

ARTICLE

POSTCRANIAL OSTEOLOGY OF THE BASALLY BRANCHING HADROSAUROID DINOSAUR *TANIUS SINENSIS* FROM THE UPPER CRETACEOUS WANGSHI GROUP OF SHANDONG, CHINA

NICLAS H. BORINDER,[*,1,8] STEPHEN F. POROPAT,[2,3,4] NICOLÁS E. CAMPIONE,[5,6,7] TOMAS WIGREN,[8] and BENJAMIN P. KEAR[8*]

[1]Geological Survey of Sweden, Fångvallsgatan 4, SE-752 37 Uppsala, Sweden, niclas.borinder@gmail.com;
[2]Faculty of Science and Technology, Swinburne University of Technology, John St, Hawthorn, Victoria 3122, Australia;
[3]Australian Age of Dinosaurs Museum of Natural History, Lot 1 Dinosaur Drive, PO Box 408, Winton, Queensland 4735, Australia;
[4]Melbourne Museum, Museums Victoria, 11 Nicholson St, Carlton, Victoria 3053, Australia, sporopat@swin.edu.au, stephenfporopat@gmail.com;
[5]Palaeoscience Research Centre, University of New England, Armidale, New South Wales, 2350, Australia;
[6]Palaeobiology Programme, Department of Earth Sciences, Uppsala University, Villavägen 16, Uppsala SE-752 36, Sweden;
[7]Department of Organismal Biology, Uppsala University, Norbyvägen 18A, Uppsala SE-752 36, Sweden, ncampion@une.edu.au;
[8]Museum of Evolution, Uppsala University, Norbyvägen 16, Uppsala SE-752 36, Sweden, tomaswigren@hotmail.com, benjamin.kear@em.uu.se

ABSTRACT—*Tanius sinensis* was one of the first dinosaur species to be named from China. It was established on a partial skeleton recovered by a joint Sino-Swedish expedition in 1923. The fossils were excavated from Upper Cretaceous strata of the Jiangjunding Formation (Wangshi Group) in Shandong Province, and although their discovery dates back almost 100 years, they have not been reassessed in detail since their initial description in 1929. This omission is critical because *T. sinensis* is now recognized as one of the stratigraphically youngest non-hadrosaurid hadrosauroid taxa. Here, we re-evaluate the postcranial osteology of *T. sinensis* as a prelude to an anatomical and phylogenetic revision of the species. We examined the holotype and all currently referred specimens of *T. sinensis* first-hand, and identified a unique postcranial character state combination incorporating tall dorsal neural spines, a reduced postacetabular ridge on the ilium, a fully enclosed flexor tunnel formed by the distal condyles of the femur, and a lunate proximal end on metatarsal III. Comparisons with other species of *Tanius* confirm that: (1) *T. chingkankouensis* is a nomen dubium erected on non-diagnostic composite material; (2) *T. laiyangensis* was established on indeterminate hadrosaurid remains that are not attributable to *Tanius*; and (3) the anecdotal assignments of *Bactrosaurus prynadai* and *Tsintaosaurus spinorhinus* to *Tanius* cannot be substantiated. Close inspection of the holotype caudal vertebra further reveals a possible healed bite trace consistent with a prey–predator interaction. Lastly, our calculated average body mass estimate for *T. sinensis* of between 2091–3533 kg suggests that it was one of the largest non-hadrosaurid hadrosauroids.

SUPPLEMENTAL DATA—Supplemental materials are available for this article for free at www.tandfonline.com/UJVP

Citation for this article: Borinder, N. H., S. F. Poropat, N. E. Campione, T. Wigren, and B. P. Kear. 2021. Postcranial osteology of the basally branching hadrosauroid dinosaur *Tanius sinensis* from the Upper Cretaceous Wangshi Group of Shandong, China. Journal of Vertebrate Paleontology. DOI: 10.1080/02724634.2021.1914642

INTRODUCTION

The first dinosaur species named from China was '*Trachodon*' *amurense* Riabinin, 1925, which was later referred to the genus *Mandschurosaurus* Riabinin, 1930, but is now regarded as a nomen dubium (sensu Horner et al., 2004). The otherwise earliest documented valid Chinese dinosaur taxa were erected by the eminent Swedish paleontologist Carl Wiman in 1929. These included the titanosauriform sauropod *Euhelopus zdanskyi* (Wiman, 1929) (see Mateer and McIntosh, 1985; Wilson and Upchurch, 2009; Poropat, 2013; Poropat and Kear, 2013a), and the hadrosauroid *Tanius sinensis* Wiman, 1929. *Tanius sinensis* was coined in honor of its discoverer, the Chinese geologist Tan Xichou, who was also often referred to (even by Tan himself) using the westernized version of his name, H. C. T'an. The remains of *T. sinensis* were recovered from Upper Cretaceous (upper Campanian–lower Maastrichtian) sediments in the Jiangjunding Formation, which is a subunit of the Wangshi Group cropping out in the Shandong peninsular region of eastern China (Hu et al., 2001; Poropat and Kear, 2013b: fig. 1; Fig. 1).

Since its initial description, the systematic relationships of *T. sinensis* have been debated. Wiman (1929) initially assigned *T. sinensis* to Hadrosauridae, a classification reiterated by Young (1958). Conversely, von Huene (1956) suggested that *T. sinensis* might constitute a separate family 'Prohadrosauridae', comprising both *T. sinensis* and *Telmatosaurus transsylvanicus* (Nopcsa, 1900). More recently, Weishampel and Horner (1990:555) listed *T. sinensis* as: "known from poor material that has yet to yield phylogenetically significant information". Nonetheless, these authors interpreted the taxon as a basally

*Corresponding authors

Published online 03 Jun 2021

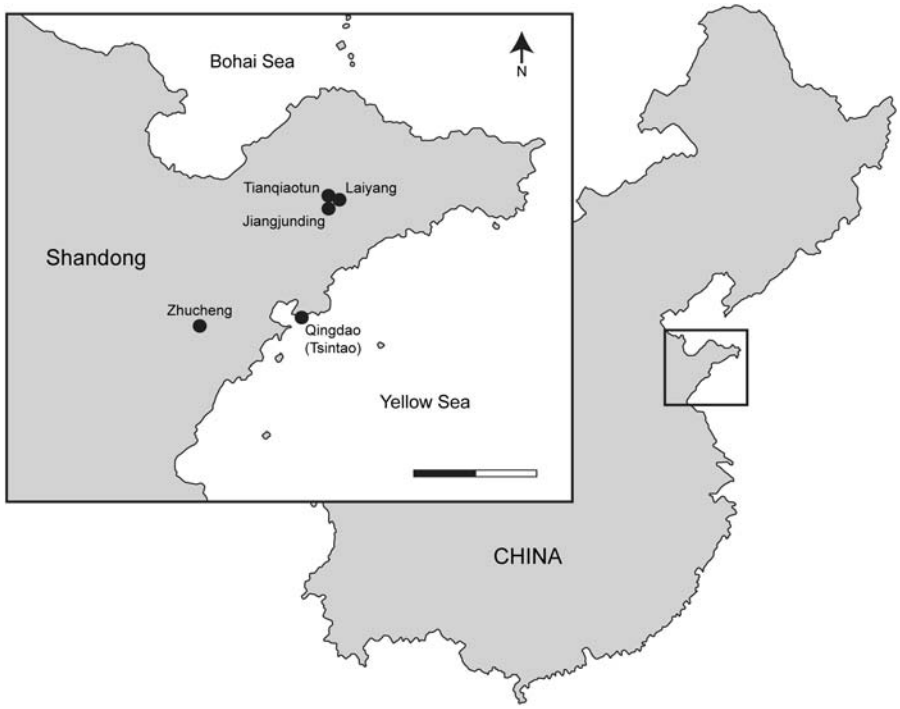

FIGURE 1. Map of the Shandong peninsular region showing source localities for the *Tanius sinensis* holotype skeleton (PMU 24720/1–32) and referred elements (PMU 22481, PMU 22482, PMU 22483, PMU 24721). Scale bar equals 100 km.

branching member of Hadrosauridae, and probably positioned amongst the sister lineages of Euhadrosauria (Lambeosaurinae + Hadrosaurinae). This proposal was predicated upon the identification of various plesiomorphic cranial traits (see discussion in Weishampel and Horner, 1990), yet the presence of tall neural spines on the dorsal vertebrae and a robust, angular deltopectoral crest on the humerus were both cited as features shared with lambeosaurines. By contrast, the phylogenetic analyses of Sues and Averianov (2009) and Prieto-Márquez and Wagner (2009) both returned *T. sinensis* as a non-hadrosaurid hadrosauroid, an affinity that has since been advocated by multiple later studies (e.g., McDonald et al., 2010; Prieto-Márquez, 2010a; McDonald, 2012; Xing et al., 2014a). This topological placement is significant because *T. sinensis* represents one of the geologically youngest non-hadrosaurid hadrosauroids. Moreover, its fossils occur in close stratigraphic proximity to those of the lambeosaurine (sensu Prieto-Márquez and Wagner, 2009) *Tsintaosaurus spinorhinus* Young, 1958, as well as the gigantic hadrosaurine (sensu Xing et al., 2014a, 2014b, 2017) *Shantungosaurus giganteus* Hu, 1973, indicating that the replacement of non-hadrosaurid hadrosauroids by hadrosaurid lineages at around the Santonian–early Campanian interval might have been exclusive to Laramidia (Norman, 2004; Evans et al., 2012; Campione et al., 2013). As a notable aside, though, Brownstein (2020) recently reported the presence of a non-hadrosaurid hadrosauroid (= 'hadrosauromorph' sensu Brownstein, 2020) from the Maastrichtian of eastern North America based on a fragmentary tibia.

Two additional species of *Tanius* Wiman, 1929 have been described since 1929: *Tanius chingkankouensis* Young, 1958; and *Tanius laiyangensis* Zhen, 1976. Nevertheless, these were variously synonymized with other taxa, or treated as nomina dubia (Buffetaut, 1995; Horner et al., 2004; Lund and Gates, 2006; Prieto-Márquez and Wagner, 2013; Zhang et al., 2020). Yet, Zhang et al. (2017) argued that *T. chingkankouensis* should be reinstated as a valid species because its scapular morphology was distinguished from that of *T. sinensis*. Moreover, the remains assigned to *T. sinensis* have received little research attention beyond literature-based comparative interpretations (Gilmore, 1933; Young, 1958; Buffetaut and Tong-Buffetaut, 1993) and phylogenies (e.g., Sues and Averianov, 2009; Prieto-Márquez and Wagner, 2009; McDonald et al., 2010; Prieto-Márquez, 2010a; McDonald, 2012; Xing et al., 2014a; McDonald et al., 2017; Zhang et al., 2020). Therefore, it is the purpose of this article to redress the shortfall in knowledge via a comprehensive reassessment of the holotype and all referred specimens of *T. sinensis*. Given the scale of such a study, we have elected to present our data as a series of papers, the first of which focuses on the postcranial skeleton and the species-level taxonomy of *Tanius*. This will be followed by a synopsis of the historically associated Wangshi Group vertebrate assemblage, and lastly a reappraisal of the cranial osteology, together with a phylogenetic revision and contextual evaluation of non-hadrosaurid hadrosauroid interrelationships.

Institutional Abbreviations—**AMNH**, American Museum of Natural History, New York, U.S.A.; **CMN**, Canadian Museum of Nature, Ottawa, Canada; **PMU**, Paleontological Collections, Museum of Evolution, Uppsala University, Uppsala, Sweden.

SYSTEMATIC PALEONTOLOGY

DINOSAURIA Owen, 1842
ORNITHISCHIA Seeley, 1887
ORNITHOPODA Marsh, 1881
IGUANODONTIA Dollo, 1888
HADROSAUROIDEA Cope, 1870
TANIUS SINENSIS Wiman, 1929
Figs. 2–12

Etymology—Wiman (1929) did not provide an etymology for *Tanius sinensis*. However, we interpret it as a Latinized combination of '*Tan-ius*', or 'belonging to Tan', which honors Tan Xichou as discoverer of the holotype; and '*sin-ensis*', referring to its geopolitical origin 'from China'.

Holotype—Wiman (1929) did not designate a specific holotype for *Tanius sinensis*, and instead treated the collective skeletal

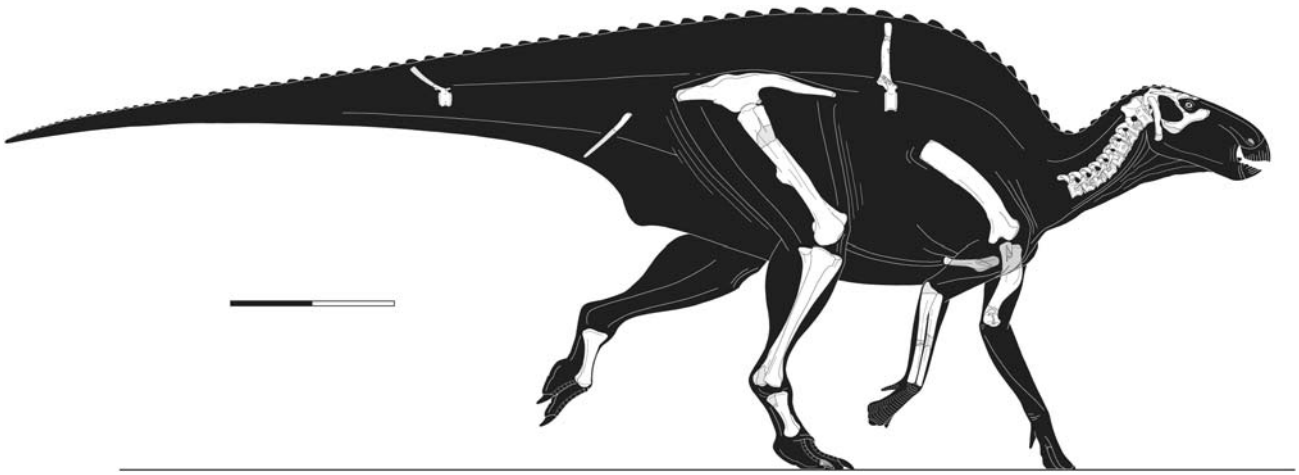

FIGURE 2. Diagrammatic reconstruction of the *Tanius sinensis* holotype skeleton (PMU 24720/1–32) in right lateral view showing life position of the recovered (white fill) and restored (darker grey fill) elements. The cranium and ilium are mirrored from the left side for completeness. Maximum body length/height as restored equals 7.84/2.83 m. Scale bar equals 1 m. Artwork © Tomas Wigren (Uppsala).

elements as a type series. Consequently, each bone was originally cataloged with separate 'PMU R' prefix numbers, which have since been superseded by a new PMU accession numbering series (see Supplemental Data 1, Table S1). Given their common provenance, as well as anatomical, ontogenetic, proportional, and morphological compatibility, we consider all of these elements as pertaining to a single individual. This skeleton has therefore been registered as PMU 24720 (Fig. 2), and incorporates an articulated skull roof and braincase (PMU 24720/1a), both postorbitals (PMU 24720/1c, PMU 24720/1d), the left jugal (PMU 24720/1b), left quadrate (PMU 24720/1h), left squamosal (PMU 24720/1e), both pterygoids (PMU 24720/1f, PMU 24720/1g), the axis and cervical vertebrae 3–10 (PMU 24720/2–10), four cervical ribs (PMU 24720/13–16; including two that articulate with the right side of cervical VI, and left side of cervical IX, respectively), a dorsal vertebra (PMU 24720/11), a mid-series caudal vertebra (PMU 24720/12), a hemal arch (PMU 24720/19), the right scapula (PMU 24720/20), right sternal plate (PMU 24720/21), left humerus (PMU 24720/22), partial right ulna (PMU 24720/23–24), proximal and distal portions of a radius (PMU 24720/25–26), the left and right ilia (PMU 24720/17, PMU 24720/18), right femur (PMU 24720/27), right tibia (PMU 24720/28), right fibula (PMU 24720/29), right metatarsal II (PMU 24720/30), left metatarsal III (PMU 24720/31), and a pedal ungual phalanx (PMU 24720/32).

Locality and Horizon—PMU 24720 was reportedly discovered approximately 500 m (= one 'li': Buffetaut, 1995) southwest of the village of Jiangjundingcun (alternately recorded as "Chiang Chün Ting" or "Chiang-Chün-Ting" on the original field labels). Additional documentation states that Jiangjundingcun was around 8 km ('16 li') southwest of the city of Laiyang (Fig. 1). This area has extensive outcrops of the Jiangjunding Formation (Wangshi Group), which are the most likely source unit for PMU 24720, and stratigraphically range from the upper Campanian to lower Maastrichtian (Xing et al., 2014b). A radiometric date of 72.9–73.5 Ma was obtained from the uppermost section of the underlying Hongtuya Formation (Yan et al., 2005), providing a maximum lower age limit for the succession.

Diagnosis—The postcranial skeleton of *Tanius sinensis* can be uniquely distinguished among non-hadrosaurid hadrosauroids by its tall dorsal neural spines (height/centrum height ratio = 3.2; proportional measurements in Supplemental Data 2, Table S2), a reduced postacetabular ridge (sensu Campione, 2014; = "caudal protuberance" sensu Prieto-Márquez, 2010a:495) on the ilium; posterior fusion of the medial and lateral distal femoral condyles to form an enclosed flexor tunnel, and a lunate profile on the proximal end of metatarsal III. The taxon also manifests a distinctive combination of other character states including: a recurved and anterodorsally directed anterior end on the scapular acromion process; maximum dorsoventral width of the proximal end of the scapula being 1.5 times that of the distal end (proportional measurements in Supplemental Data 2, Table S3); a strongly curved dorsal margin on the scapula; a deltopectoral crest less than 50% of the maximum length of the humerus; an expanded 'club-like' distal end on the fibula; central plate of the ilium with a depth/length ratio = 0.91; and the proximodistal length of metatarsal III being 4.5 times greater than its mid-shaft width.

Comments—Wiman (1929) mentioned that the PMU 24720 skeleton was largely complete when found, but that many bones (including the rostral section of the skull) disintegrated during excavation and could not be retrieved. Indeed, the remaining elements are extremely fragile and require continual conservation. PMU archive documents report that Tan Xichou initially collected the cervical vertebrae and some other postcranial remains on April 20, 1923 (see also Wiman, 1929). Additional components of the skeleton were then recovered throughout October 1923 by the Austrian paleontologist, Otto Zdansky, who was commissioned to explore for fossils in China on behalf of Uppsala University. Wiman (1929:49) further noted that the caudal vertebra PMU 24720/12 was separated from the rest of the skeleton, and occurred in conjunction with various theropod and sauropod bones (Poropat, 2013; Poropat and Kear, 2013b). However, its morphological and proportional compatibility supports attribution to the type series. Wiman (1929) also described an isolated dorsal rib (PMU 22481) discovered around 2.5 km ('five li') southwest of Jiangjundingcun, together with a right humerus (PMU 24721), radius (PMU 22483) and metatarsal (PMU 22482), all collected northeast of the village of Tianqiaocun (transcribed as 'T'ien Ch'iao T'un'), 1.5 km to the northwest of Jiangjundingcun. Nevertheless, these specimens are not diagnostic beyond Hadrosauroidea indet., and are thus excluded from the holotype material herein. Lastly, Wiman (1929) documented the distal section of a right ischium (PMU 22485), which was later recognized as part of a theropod left pubis (Gilmore, 1933; Buffetaut and

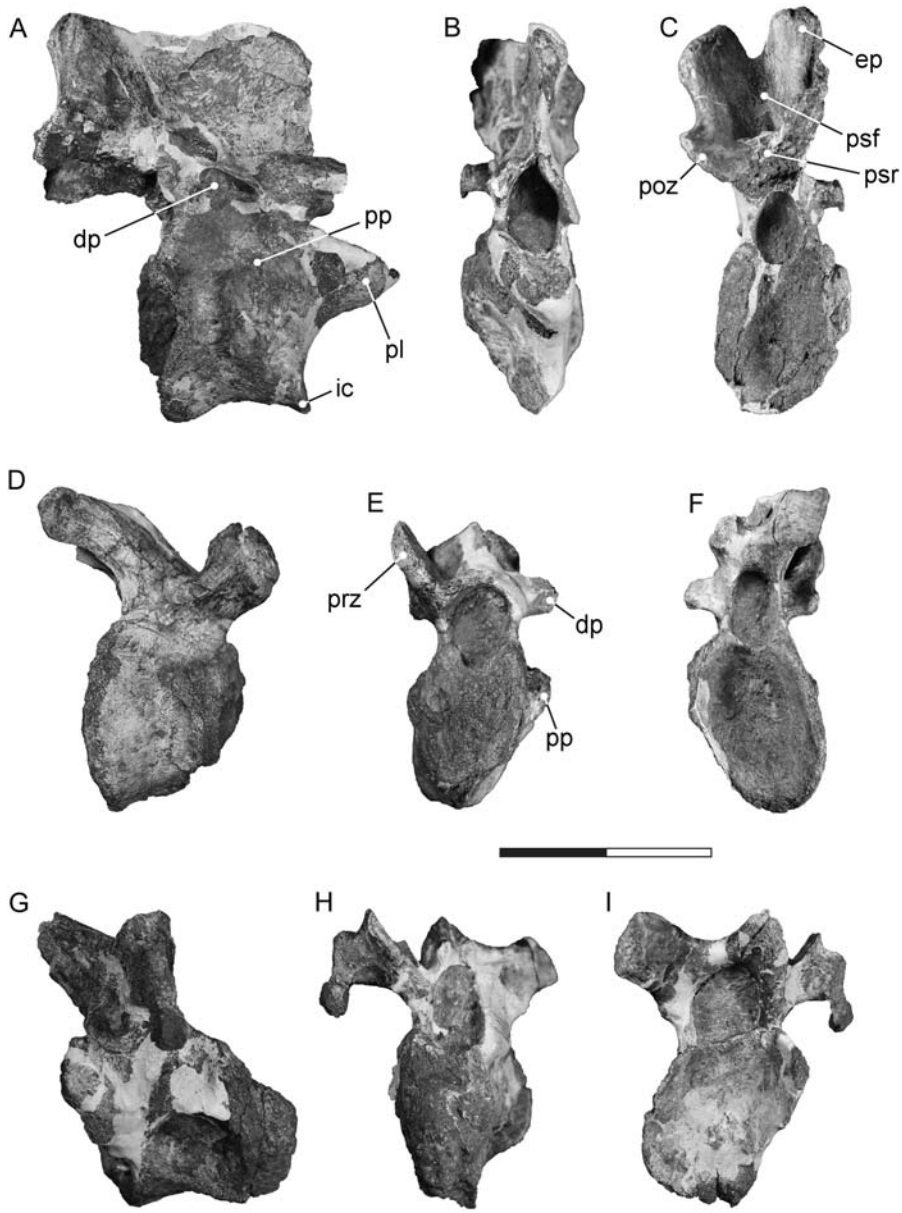

FIGURE 3. *Tanius sinensis* holotype cervical vertebrae. Axis (PMU 24720/2) in **A**, lateral, **B**, anterior, and **C**, posterior view. Cervical 3 (PMU 24720/3) in **D**, lateral, **E**, anterior, and **F**, posterior view. Cervical 4 (PMU 24720/4) in **G**, lateral, **H**, anterior, and **I**, posterior view. Scale bar equals 100 mm. **Abbreviations**: **dp**, diapophysis; **ep**, epipophysis; **ic**, intercentrum; **pl**, pleurocentrum; **poz**, postzygapophysis; **pp**, parapophysis; **prz**, prezygapophysis; **psf**, post-spinal fossa; **psr**, post-spinal ridge.

Tong-Buffetaut, 1993). We also identified a corresponding right pubis (PMU 22484) that, together with PMU 22485, are likely attributable to a tyrannosauroid (Supplemental Data 1, Table S1), but will be documented in more detail elsewhere.

DESCRIPTION OF THE POSTCRANIAL SKELETON

Axial Skeleton

Cervical Vertebrae—The disarticulated cervical series comprises the axis (C2) and cervical vertebrae 3–10 (C3–10). All of the vertebrae were diagenetically distorted. The cervical vertebrae are opisthocoelous, like those of other hadrosauroids (Horner et al., 2004). The post-axial neural spines form low ridges, or become knob-like in C6. The prezygapophyses are triangular in cross-section and situated dorsally on the transverse processes; they extend posterolaterally beyond the posterior articular surfaces when viewed in dorsal aspect. A horizontal ridge extends across the lateral surfaces of some centra, which is similar to the cervicals of *Bactrosaurus johnsoni* (Godefroit et al., 1998) and *Eolambia caroljonesa* Kirkland, 1998 (McDonald et al., 2012a); this ridge becomes more pronounced in the posterior cervicals, but is accentuated by crushing.

The axis (Fig. 3A–C) is transversely compressed and its left side is reconstructed in plaster. The atlantal pleurocentrum (= odontoid) is fused to the axial centrum. Its dorsal surface is horizontally oriented with a shallow concavity that accommodates the neural canal. The ventral surface is diagonally offset relative to the centrum, imparting a keeled lateral profile that is reminiscent of the axis in *Iguanodon bernissartensis* Boulenger, 1881 (Norman, 1980); the ventral margin is otherwise more rounded in *B. johnsoni* and other hadrosauroids (Prieto-Marquez, 2007; Ramírez-Velasco et al., 2012). Horner et al. (2004) stated that the atlantal pleurocentrum remains unfused in all hadrosaurids. However, this assertion was based on an osteologically immature

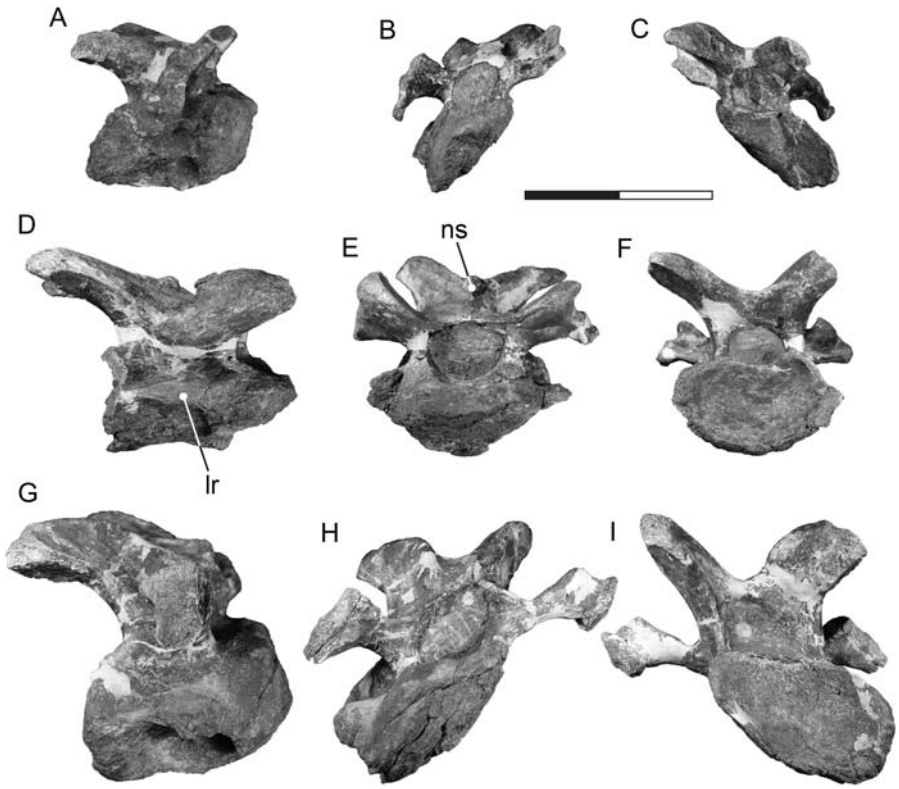

FIGURE 4. *Tanius sinensis* holotype cervical vertebrae. Cervical 5 (PMU 24720/5) in **A**, lateral, **B**, anterior, and **C**, posterior view. Cervical 6 (PMU 24720/6) in **D**, lateral, **E**, anterior, and **F**, posterior view. Cervical 7 (PMU 24720/7) in **G**, lateral, **H**, anterior, and **I**, posterior view. Scale bar equals 100 mm. **Abbreviations**: **lr**, lateral ridge; **ns**, neural spine.

specimen of *Gryposaurus notabilis* Lambe, 1914 (Prieto-Márquez, 2010b); the atlantal pleurocentrum is otherwise usually fused to the axis in hadrosauroids (Norman, 1980; Maryańska and Osmólska, 1984; Evans and Reisz, 2007; Prieto-Marquez, 2007).

A wedge-shaped intercentrum is fused to the anteroventral articulation surface of the axial pleurocentrum. The posterior articular surface of the axis is concave and oval, with a dorsal notch for the neural canal. The parapophysis is robust and dorsoventrally elongate. The posterolateral centrum surface is smooth with nutrient foramen that is 5 mm in maximum diameter. The neural arch and centrum are fused without trace of a neurocentral suture. The projecting right diapophysis is laterally tapered with an oval distal outline; it is situated at the same level as the prezygapophyses, unlike *B. johnsoni* where the diapophysis is more posteroventrally oriented (Godefroit et al., 1998). The prezygapophyses extend anteriorly in front of the dorsolaterally inclined articular facets.

The axial neural spine is transversely compressed (minimum width = 11 mm) and has smooth lateral surfaces. The anterior margin is broken but likely projected forwards. The dorsal edge has been restored, but was apparently tallest above the postzygapophyses, and lacks any obvious embayment like the axial neural spines of many hadrosaurines (Campione et al., 2007; Prieto-Márquez, 2010a).

The axial postzygapophyses are ventrolaterally oriented and diverge from a common base that overhangs the posterior articulation surface; this roofs the neural canal and forms the ventral margin of the post-spinal fossa. The post-spinal fossa is defined laterally by tall epipophyses that extend dorsally from the postzygapophyses. A small post-spinal ridge is situated within the fossa and extends about one-third the height of the epipophyses, as preserved. The post-spinal fossa imparts a Y-shape to the dorsal margin of the axial neural spine. Gasca et al. (2015) recorded an axial spine height/length ratio of 43%; however, we consider this ambiguous because the specimen is incomplete.

The post-axial cervicals C3–C10 (Figs. 3D–I, 4A–I, 5A–I) are opisthocoelous with extremely reduced neural spines. The parapophyses are located on the lateral sides of the centra and border the posterior edges of the anterior articular surfaces. Where intact, the parapophyseal apices are circular to oval in outline and laterally projecting. The left parapophysis of vertebra C4 is situated along the mid-line of the centrum, slightly more posteriorly than that of C3. The parapophyses of C6 and C7 are positioned lower on the centra than those of the other cervicals, but this may be a result of distortion.

An anteroposteriorly elongate lateral ridge is present on C4–C10 and buttresses the parapophysis anteriorly to delimit paired dorsal and ventral fossae. The lateral ridges become more pronounced posteriorly, although this is exaggerated by crushing. An anteroposterior keel is also present on the ventral surface of the centrum in C3. In C4, the ventral fossa is flanked by two anteroposteriorly oriented ridges. In C8 (but possibly also in C5–7), the ventral fossa is reduced, and the ventral surface becomes planar.

The posterior articular surfaces of the centra in C3–C8 are transversely broad and dorsoventrally tall, imparting a heart-shaped profile. By contrast, C9 and C10 are ovate in outline. The centra of C3–C7 become increasingly compact in lateral view, unlike those of C8 and C10, which are rhombic. The anterior articulation surface of C10 is angled posteriorly. Nutrient foramina are visible on the ventral surfaces of C3 and C6, but were probably present on all of the cervical vertebra in life.

The post-axial cervical neural arches are tall and enclose neural canals that increase in diameter posteriorly; in C6 and

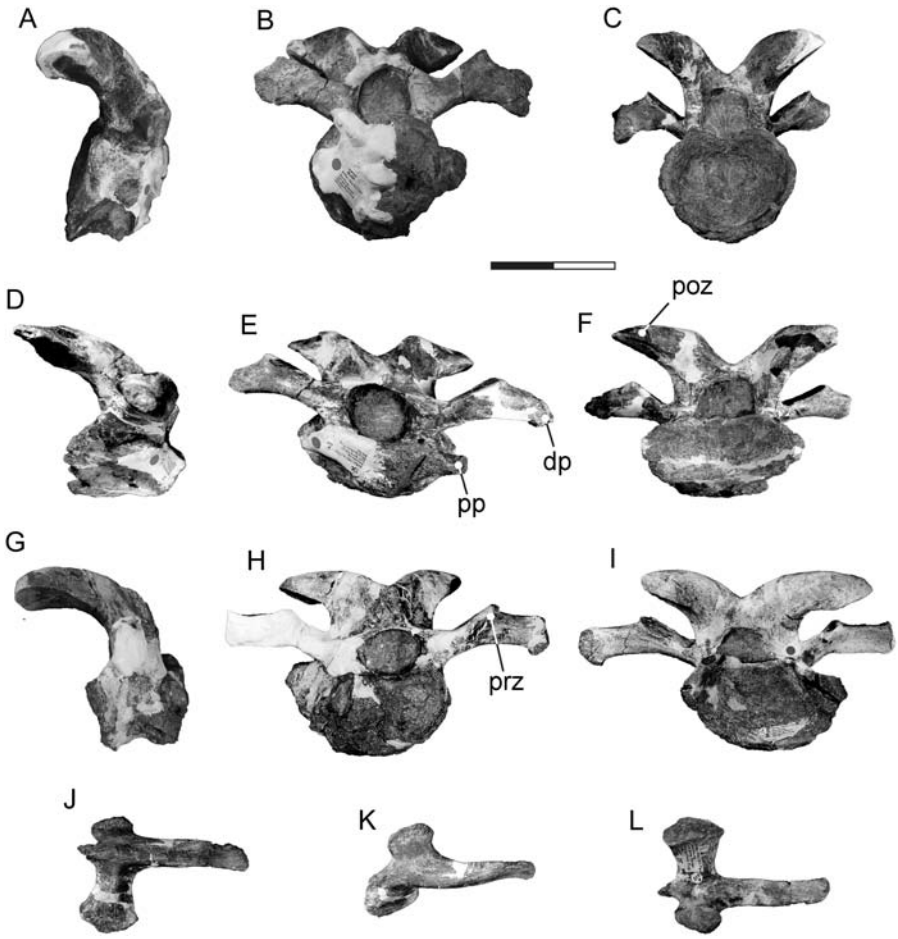

FIGURE 5. *Tanius sinensis* holotype cervical vertebrae and ribs. Cervical 8 (PMU 24720/8) in **A**, lateral, **B**, anterior, and **C**, posterior view. Cervical 9 (PMU 24720/9) in **D**, lateral, **E**, anterior, and **F**, posterior view. Cervical 10 (PMU 24720/10) in **G**, lateral, **H**, anterior, and **I**, posterior view. Cervical rib IX (PMU 24720/14) in **J**, ventrolateral, **K**, dorsolateral, and **L**, ventromedial view. Scale bar equals 100 mm. **Abbreviations**: **dp**, diapophysis; **poz**, postzygapophysis; **pp**, parapophysis; **prz**, prezygapophysis.

C7, the anterior opening is transversely wider than that of C8, but this is likely due to distortion. The neural spines form low ridges and are knob-like in C6.

The prezygapophyses are broader than long and have dorsomedially angled articular facets; this changes to a more horizontal orientation with the prezygapophyses becoming increasingly divergent in the posterior cervicals. The prezygapophyses contact the diapophyses at their base, and together support the transverse processes. Unusually, the posterior margin of the right prezygapophysis on C3 bears a deep excavation, which does not appear to be pathological.

The postzygapophyseal processes extend posterolaterally and are triangular in cross-section. Their articular facets are ventrolaterally oriented, but more horizontally facing on C10. A distally sloping ridge extends along the dorsal surface of each postzygapophyseal process and becomes medially oriented throughout the cervical column. A post spinal fossa is present between the postzygapophyseal processes on C2 but is less evident in subsequent vertebrae.

Where preserved, the transverse processes on the post-axial cervicals are long and robust, resembling those of *E. caroljonesa* (McDonald et al., 2012a) and *Edmontosaurus regalis* Lambe, 1917 (Campione, 2014). The diapophyses contact the base of the neural arch via a buttress, situated near the posteroventral margin of each transverse process in C3–C6, but shifted towards the anteroventral margin in C7–C10. The diapophyseal articular surfaces are circular to oval in outline, and ventrolaterally to laterally oriented along the column, but nearly horizontal in C10.

Cervical Ribs—Of the four recovered cervical ribs, Wiman (1929) identified PMU 24720/13 as being from the right side of C6 and PMU 24720/14 from the left side of C9 (Fig. 5J–L). All of the ribs possess a posteriorly directed prong-like shaft, which, together with the capitulum and tuberculum, diverge at about a 90° angle from the proximal end. Broken remnants of the tubercula are also preserved in articulation with the diapophyses on C4 and C6. A short spur-like process projects anteriorly from between the capitulum and tuberculum on each rib. The posterior section of the shaft is otherwise straight to slightly curved in lateral view and flat to concave in medial view. A ridge extends from the anterior process along the shaft for around one-third of its total length. The tuberculum and the capitulum terminate in anteroposteriorly expanded convex contacts for the diapophysis and parapophysis, respectively.

Dorsal Vertebra—The only recovered dorsal vertebra, PMU 24720/11, is virtually complete except for the distal-most extremity of the left transverse process (Fig. 6A–C). The centrum is amphiplatyan with a flat anterior articular surface and a shallowly concave posterior articular surface. The anterior articular surface is 96/99 mm in maximum height/width and has a circular profile. The posterior articular surface is 110/96 mm in maximum height/width and more heart-shaped in outline because of its inset dorsal margin bordering the neural canal. The lateral surfaces of the centrum are pierced by nutrient foramina and converge medially to form a weak ventral keel.

The neurocentral sutures are visible but fully fused. The neural arch pedicles enclose a dorsoventrally tall neural canal. The

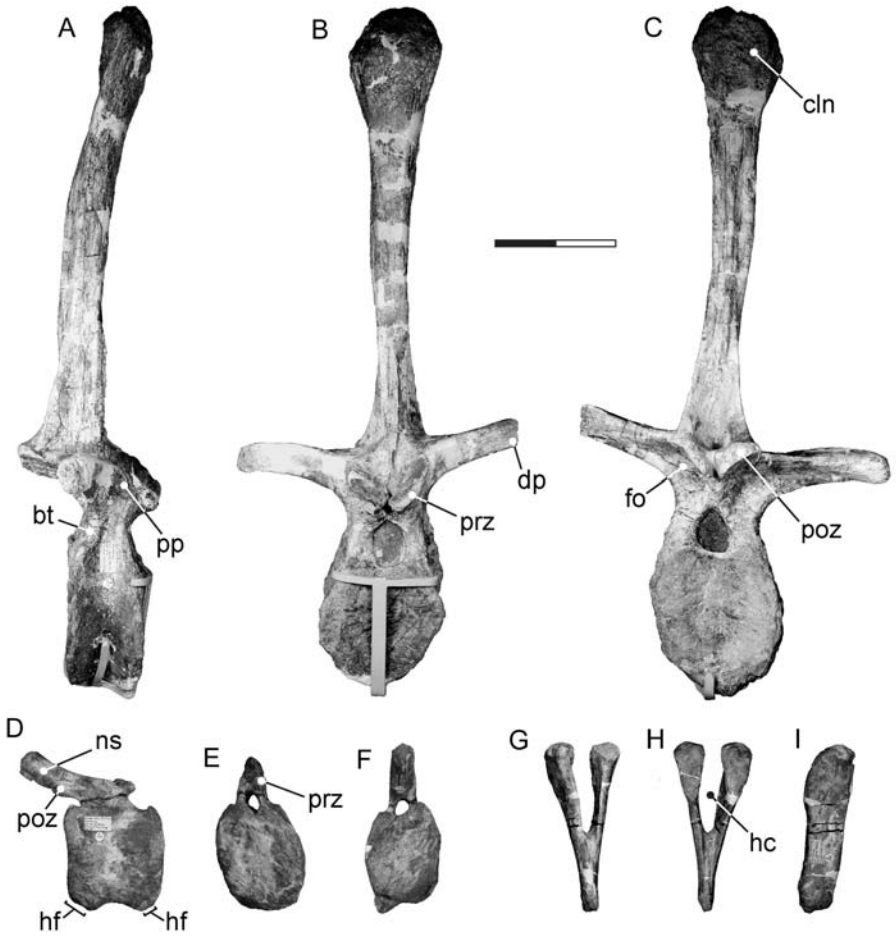

FIGURE 6. *Tanius sinensis* holotype dorsal vertebra, caudal vertebra, and hemal arch. Dorsal vertebra (PMU 24720/11) in **A**, lateral, **B**, anterior, and **C**, posterior view. Caudal vertebra (PMU 24720/12) in **D**, lateral, **E**, anterior, and **F**, posterior view. Hemal arch (PMU 24720/19) in **G**, anterior, **H**, posterior, and **I**, lateral view. Scale bar equals 100 mm. **Abbreviations**: **bt**, buttress; **cln**, club-like apex on the neural spine; **dp**, diapophysis; **fo**, fossa; **hc**, hemal canal; **hf**, hemal arch facet; **ns**, neural spine; **poz**, postzygapophysis; **pp**, parapophysis; **prz**, prezygapophysis.

parapophyseal articular surface is flush with the lateral surface of the neural arch and situated adjacent to the anterior base of the transverse process between the prezygapophysis and diapophysis. A thin ridge connects the lateral margin of the prezygapophyseal facet with the dorsal margin of the transverse process.

The transverse processes project perpendicularly relative to the vertical axis of the dorsal vertebra. Their anterior surfaces are flat, but become shallowly concave dorsally. A stout buttress extends along the ventral surface to the base of the neural arch and delimits a shallow triangular fossa that can be observed in posterior view. The maximum mediolateral width of the less distorted right transverse process is 130 mm when measured from the vertical midline of the vertebra.

The dorsal prezygapophyses are situated at the base of the neural spine. The prezygapophyseal facets are dorsomedially oriented and separated along their mid-line. The corresponding postzygapophyseal facets are ventrolaterally oriented and likewise medially separated. Stout buttresses extend ventrally from the postzygapophyses to diverge around the neural canal. Narrow ridges also ascend from the postzygapophysis along the posterolateral margins of the neural spine, and define a small fossa that terminates in a ridge extending along approximately two-thirds of the vertical height of the posterior edge towards the neural spine apex.

The dorsal neural spine is 346/359 mm in maximum height as measured from the base of the left/right transverse process, respectively. The posterior margin is 110 mm in maximum height, yielding a neural spine to centrum ratio of 3.2; Prieto-Márquez (2011b) alternatively estimated a ratio of 3.7. The dorsal neural spines of hadrosaurs often increase in height along the vertebral column (Horner et al., 2004; but see Campione, 2014), and the corresponding centra become anteroposteriorly compressed (Godefroit et al., 1998; Campione, 2014); this is comparable to the posterior dorsals of *Eolambia caroljonesa* and *Edmontosaurus regalis* (McDonald et al., 2012a; Campione, 2014). The neural spine of PMU 24720/11 is otherwise more gracile than those of iguanodontians, such as *Ouranosaurus nigeriensis* Taquet, 1976 and *Morelladon beltrani* Gasulla, Escaso, Narváez, Ortega and Sanz, 2015, or the hadrosaurids *Hypacrosaurus altispinus* Brown, 1913 (Prieto-Márquez, 2011b), *Barsboldia sicinskii* Maryańska and Osmólska, 1981, and *Magnapaulia laticaudus* (Morris, 1981) (see Prieto-Márquez et al., 2012).

The distal extremity of the dorsal neural spine is expanded into a 'club-like' apex, which is 74/43 mm in maximum transverse width/anteroposterior length, respectively. Similar 'club-like' neural spine apices occur in *Bactrosaurus johnsoni*, *Gilmoreosaurus mongoliensis* (Gilmore, 1933), and *B. sicinskii* (Godefroit et al., 1998; Prieto-Márquez and Norell, 2010; Prieto-Márquez, 2011b). The dorsal-most apical surface of the neural spine is rugose and was probably covered by cartilage in life. The lateral apical surfaces are shallowly concave and ornamented by striations. The anterior apical surface is transversely convex but becomes progressively flattened distally.

Caudal Vertebra—We interpret PMU 24720/12 (Fig. 6D–F) as deriving from the mid-caudal series based on comparisons with

FIGURE 7. *Tanius sinensis* holotype pectoral girdle elements. Right scapula (PMU 24720/20) in **A**, lateral and **B**, medial views. Right sternal plate (PMU 24720/21) in **C**, dorsal, **D**, lateral, **E**, ventral, and **F**, medial views. Scale bar equals 200 mm. **Abbreviations**: **ap**, acromion process; **ca**, coracoids articulation; **dr**, deltoid ridge; **gla**, glenoid articulation.

Iguanodon bernissartensis, *Bactrosaurus johnsoni*, *Eolambia caroljonesa*, and *Edmontosaurus regalis* (Norman, 1980; Godefroit et al., 1998; McDonald et al., 2012a; Campione, 2014). Its centrum is slightly amphicoelous, resembling the caudals of *E. caroljonesa* (McDonald et al., 2012a), but differing from the anterior to mid-series caudal vertebrae of *I. bernissartensis* (Norman, 1980) and *E. regalis* (Campione, 2014), which are platycoelous to amphiplatyan, respectively. The centrum of PMU 24720/12 is also slightly higher than long, with hemal arch facets on both the anteroventral and posteroventral edges. The posterior hemal articular facets are especially deeply inset and separated by a midline prominence. The ventral surface of the centrum is concave and bordered ventrolaterally by longitudinal ridges.

The right prezygapophysis of PMU 24720/12 has broken off, and the left prezygapophysis is incomplete. Nonetheless, both were evidently small, with a maximum mediolateral width equivalent to that of the adjacent neural canal. The corresponding postzygapophyses are similarly reduced and do not appear to have projected over the succeeding vertebra. Low ridges extend from the prezygapophyses and merge along the anterior edge of the neural spine, which is posteriorly inclined like those of *I. bernissartensis*, *B. johnsoni*, and *E. caroljonesa* (Norman, 1980; Godefroit et al., 1998; McDonald et al., 2012a); this inclination becomes more extreme in the posterior-most caudal vertebrae of *E. regalis* (Campione, 2014).

Hemal Arch—The recovered hemal arch PMU 24720/19 (Fig. 6G–I) has a maximum proximodistal length of 152 mm, a maximum depth of the hemal canal at 74 mm, and a maximum width between the proximal facets of 43 mm. In general form, PMU 24720/19 resembles the more anterior hemal arches of *Iguanodon bernissartensis*, *Eolambia caroljonesa*, and *Edmontosaurus regalis* (Norman, 1980; McDonald et al., 2012a; Campione, 2014). The hemal spine of PMU 24720/19 is incomplete but the anterior and posterior surfaces are concave with a thin vertical midline ridge visible posteriorly. The proximal facets are borne on transversely narrow hemal processes, which enclose the hemal canal. Each facet surface is anteroposteriorly elongate and oval in outline with a posterodorsal inflection, suggesting that the hemal arch was probably posteroventrally angled when articulated with the corresponding caudal centra.

Appendicular Skeleton

Scapula—The recovered right scapula PMU 24720/20 is elongate, blade-like, and posteriorly curved in lateral view (Fig. 7A, B). This condition is closely comparable with some other non-hadrosaurid hadrosauroids, such as *Telmatosaurus transylvanicus*, *Tethyshadros insularis* Dalla Vecchia, 2009, and *Zhanghenglong yangchengensis* Xing, Wang, Han, Sullivan, Ma, He, Hone, Yan, Du, and Xu, 2014a (Dalla Vecchia, 2006, 2009; Xing et al. 2014a). A similar but less strongly curved scapula also occurs in *Iguanodon bernissartensis*, *Jinzhousaurus yangi* Wang and Xu, 2001, and *Magnamanus soriaensis* Fuentes Vidarte, Meijide Calvo, Meijide Fuentes, and Meijide Fuentes, 2016 (Norman, 1980; Wang et al., 2011; Fuentes Vidarte et al. 2016).

The scapular blade of PMU 24720/20 is uniformly wide along its length with a distinctly rectangular distal end, as in *I. bernissartensis*, *Eolambia caroljonesa*, and *Edmontosaurus regalis* (Norman, 1980; McDonald et al., 2012a; Campione, 2014); although this contrasts with *Bactrosaurus johnsoni* and *Z. yangchengensis* in which the distal extremity is less expanded (Godefroit et al., 1998; Xing et al., 2014a).

The acromion process is prominent and anterodorsally recurved unlike those of *B. johnsoni*, *Gilmoreosaurus mongoliensis*, *Z. yangchengensis*, *Nanningosaurus dashiensis* Mo, Zhao, Wang, and Xu, 2007, and *Gobihadros mongoliensis* Tsogtbaatar, Weishampel, Evans, and Watabe, 2019 (Godefroit et al., 1998; Prieto-Márquez and Norell, 2010; Xing et al., 2014a; Tsogtbaatar et al., 2019). The deltoid ridge extends distally from the acromion process and merges laterally with the scapular blade, as occurs in *B. johnsoni*, *E. caroljonesa*, and *E. regalis* (Godefroit et al., 1998; McDonald et al., 2012a; Campione, 2014); however, the deltoid ridges in *B. johnsoni* and *E. regalis* are not as well defined, and alternatively form low swellings that border the deltoid fossa dorsally (McDonald et al., 2012a; Campione, 2014).

The proximal articular surface of PMU 24720/20 supports both the glenoid and coracoid contact. Its maximum dorsoventral

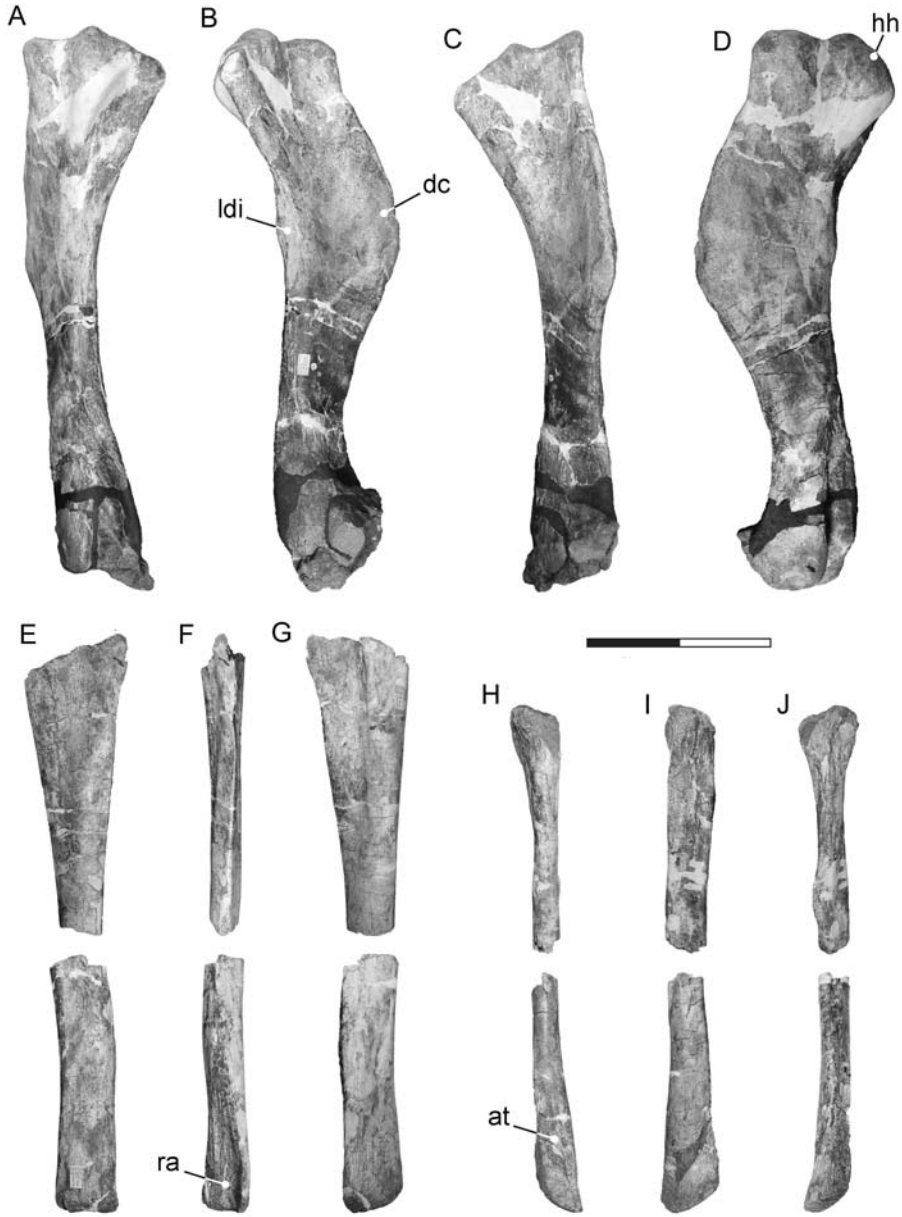

FIGURE 8. *Tanius sinensis* holotype forelimb elements. Left humerus (PMU 24720/22) in **A**, posterior, **B**, medial, **C**, anterior, and **D**, lateral view. Right proximal (PMU 24720/23) and distal (PMU 24720/24) sections of the ulna in **E**, anterior, **F**, medial, and **G**, posterior view. Right proximal (PMU 24720/25) and distal (PMU 24720/26) sections of the radius in **H**, anterior, **I**, medial, and **J**, posterior view. Scale bar equals 200 mm. **Abbreviations**: **at**, anterior trough; **dc**, deltopectoral crest; **hh**, humeral head; **ldi**, m. latissimus dorsi insertion; **ra**, radial articulation.

height exceeds that of the distal extremity of the scapula, which is similar to most non-hadrosaurid hadrosauroids, except for *B. johnsoni* (Godefroit et al., 1998). The deltoid ridge of PMU 24720/20 is less robust than that of *B. johnsoni* (Prieto-Márquez, 2011a), but this trait is influenced by ontogeny (Brett-Surman and Wagner, 2007) and thus might reflect the relative osteological maturity of the *T. sinensis* holotype individual.

Sternal Plate—The right sternal plate, PMU 24720/21, lacks its anterior-most end (Fig. 7C–F) but clearly possesses a classic 'hatchet-shaped' outline typical of hadrosauroids (Norman, 2004). Its shaft is short and stocky with a D-shaped cross-section formed by the rounded ventral and flattened dorsal surfaces. The dorsal surface becomes progressively more concave towards the expanded anterior end. The distal end is rugose and elliptical in outline with a medial deflection relative to the long axis of the bone. Conversely, the distal extremity of the sternal plate is dorsoventrally flattened in *Edmontosaurus regalis* (Campione, 2014), or distinctly faceted in *Probactrosaurus gobiensis* Rozhdestvensky, 1966 (see also Rozhdestvensky, 1967 for an English translation) and *Bactrosaurus johnsoni* (Godefroit et al., 1998; Norman, 2002). In comparison, the shaft of the sternal plate in PMU 24720/21 is shorter and broader than that of *B. johnsoni* (Godefroit et al., 1998), but this can vary intraspecifically in ornithopods (Brett-Surman and Wagner, 2007; Verdú et al., 2017; Prieto-Márquez and Guenther, 2018).

Humerus—The left humerus, PMU 24720/22 (Fig. 8A–D), has a sinuous profile and a mediolaterally broad proximal end with a medially offset humeral condyle. The lateral and proximal margins of the humerus form an obtuse angle, as evident in *Eolambia caroljonesa* and *Edmontosaurus regalis* (McDonald, 2012; Campione, 2014), but unlike the more perpendicular angle of the proximal humerus in *Iguanodon bernissartensis* (Norman, 1980). The prominent deltopectoral crest of PMU 24720/22 extends about 40% of the maximum distance along

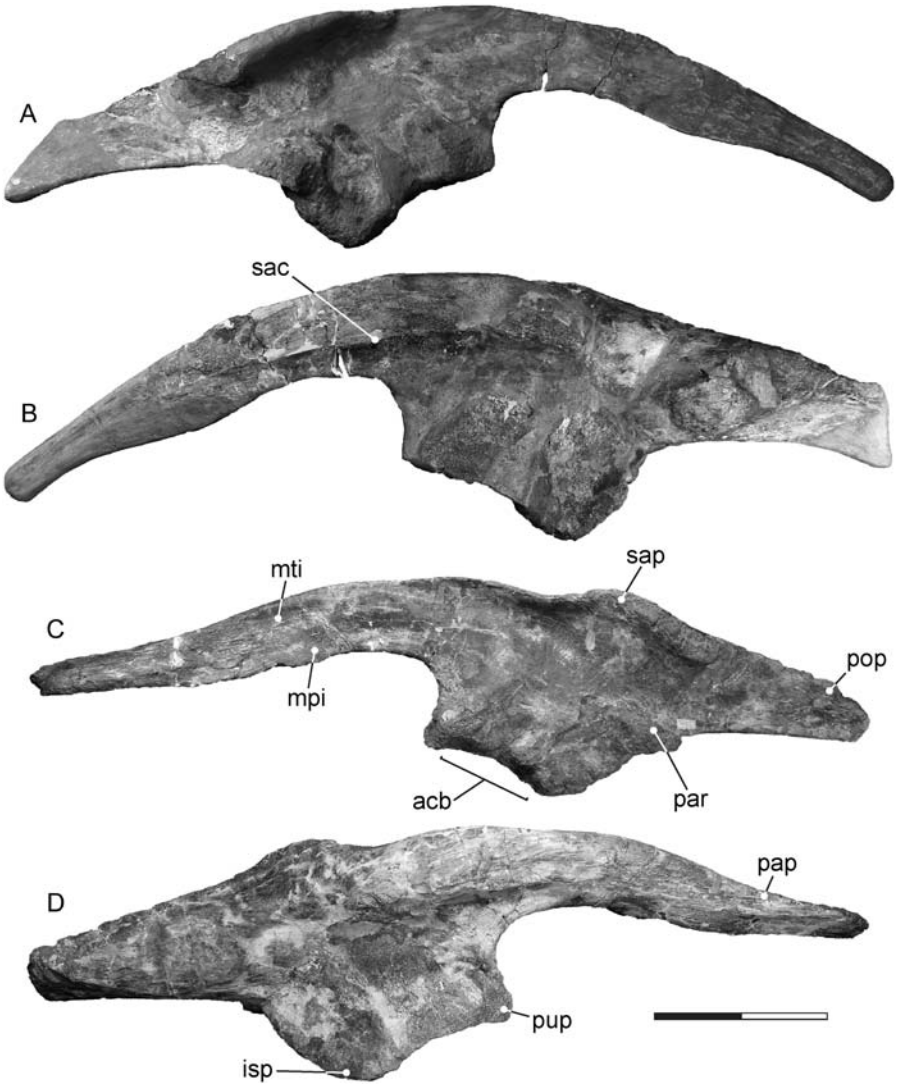

FIGURE 9. *Tanius sinensis* holotype pelvic girdle elements. Right ilium (PMU 24720/17) in **A**, lateral and **B**, medial view. Left ilium (PMU 24720/18) in **C**, lateral and **D**, medial view. **Abbreviations**: **acb**, acetabulum; **isp**, ischial peduncle; **mpi**, m. puboischiofemoralis internis insertion; **mti**, m. iliotibialis insertion; **pap**, preacetabular process; **par**, postacetabular ridge; **pop**, postacetabular process; **pup**, pubic peduncle; **sac**, sacral articulation: **sap**, supraacetabular process.

the humeral shaft and has a flattened lateral margin. Corresponding deltopectoral crest lengths of less than 50% are typical of non-hadrosaurid hadrosauroids, although this may be affected by ontogeny (Dilkes, 2001; Egi and Weishampel, 2002; Verdú et al., 2017). The shape of the deltopectoral crest in PMU 24720/22 is otherwise similar to those of *Bactrosaurus johnsoni* (Godefroit et al., 1998) and *Nanyangosaurus zhugeii* Xu, Zhao, Lü, Huang, Li, and Dong, 2000, yet is not as ventrally constricted or apically tapered as that of *N. zhugeii* (Xu et al., 2000).

The humeral shaft of PMU 24720/22 bears a small posterior prominence for attachment of the m. latissimus dorsi (see Campione, 2014). In addition, despite being partially encased in matrix, the medial and lateral condyles on the distal extremity are visibly sub-equal in size and separated by deep intercondylar grooves.

Ulna—The right ulna is broken into proximal (PMU 24720/23) and distal (PMU 24720/24) sections (Fig. 8E–G), and lacks most of the olecranon process. Nonetheless, its general morphology is consistent with the ulnae of other hadrosauroids (Norman, 2004; Horner et al., 2004). A distally tapering trough is present on the anterior and posterior surfaces, and the proximal end of the shaft has an irregular 'T-shaped' cross-section similar to that reported in *Edmontosaurus regalis* (Campione, 2014). By contrast, the distal end of the shaft is elliptical in cross-section with a maximum diameter of 43 mm. The distal-most articulation surface is convex and highly rugose indicating the presence of cartilage.

Radius—Like the ulna, the right radius is broken into proximal (PMU 24720/25) and distal (PMU 24720/26) sections (Fig. 8H–J) and has been mediolaterally compressed during diagenesis. Nonetheless, the shaft is visibly sub-trapezoidal in cross-section, and has a concave laterally sloping proximal articular surface that is bordered by a low posterior flange. The shaft of the radius is straight and anteroposteriorly flattened with a tapering anterior trough that expands distally. The distal articular surface is convex and rugose with a triangular outline in distal view.

Ilium—Both the left (PMU 24720/17) and right ilia (PMU 24720/18) were recovered, although the right ilium has been extensively reconstructed in plaster (Fig. 9A, B). The better preserved left ilium (Fig. 9C, D) has a sigmoidal dorsal profile in lateral view, as in *Bactrosaurus johnsoni* (Godefroit et al., 1998), but differs from the otherwise straighter ilia in most basally branching hadrosauroids, such as *Eolambia caroljonesa*

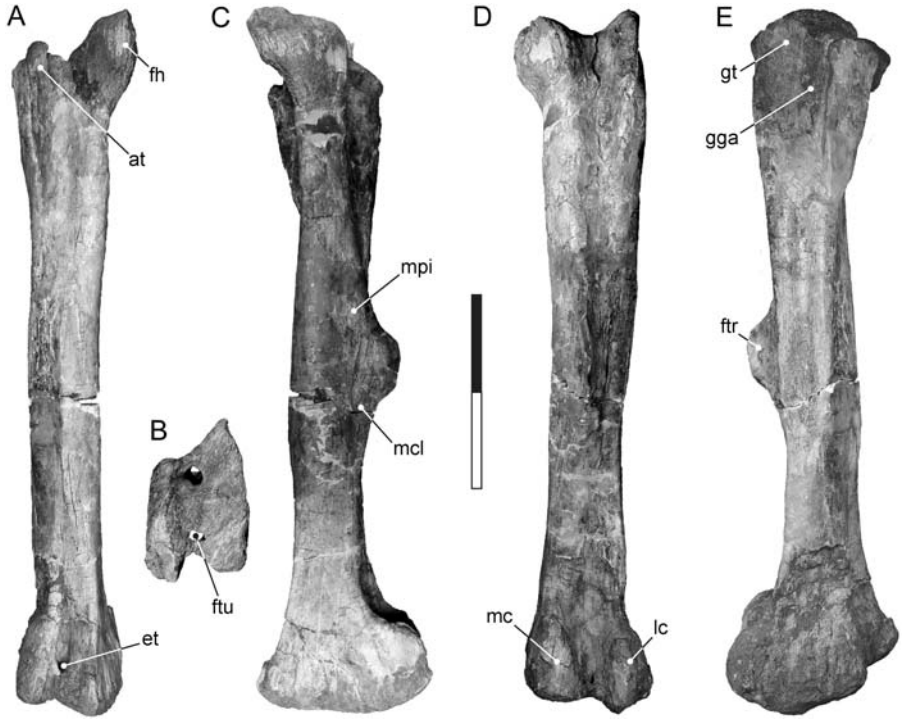

FIGURE 10. *Tanius sinensis* holotype right femur (PMU 24720/27) in **A**, anterior, **B**, distal articular, **C**, medial, **D**, posterior, and **E**, lateral views. Scale bar equals 200 mm. **Abbreviations**: **at**, anterior trochanter; **et**, extensor tunnel; **fh**, femoral head; **ftu**, flexor tunnel; **ftr**, fourth trochanter; **gt**, greater trochanter; **gga**, groove separating the greater and anterior trochanters; **lc**, lateral condyle; **mc**, medial condyle; **mcl**, m. caudofemoralis longus insertion; **mpi**, m. puboischiofemoralis internis insertion.

and *Zuoyunlong huangi* Wang, You, Wang, Xu, Yi, Xie, Jia, and Xing, 2017 (McDonald et al., 2012a; Wang et al., 2017). Moreover, it is noticeably less robust than the ilia of *B. johnsoni* (Godefroit et al., 1998) and lacks the conspicuous dorsoventral expansion of the preacetabular process evident in *Iguanodon bernissartensis* and *E. caroljonesa* (Norman, 1980; McDonald et al., 2012a).

The preacetabular process of PMU 24720/17 curves ventrally but is less deflected than those of *I. bernissartensis* and *B. johnsoni* (Norman, 1980; Godefroit et al., 1998; Verdú et al., 2017); this is alternatively reminiscent of *Edmontosaurus regalis* (Campione, 2014) the preacetabular process of which is similarly elongate relative to the maximum length of the ilium. An anteroposteriorly elongate ridge extends from the preacetabular process to around the midpoint of the dorsal third of the central plate (contra Prieto-Márquez and Norell, 2010), and corresponds to the attachment area for the sacral ribs.

The pubic peduncle of PMU 24720/17 is blunt, triangular, and does not align with the ischial peduncle when the ilium is oriented in life position. The pubic peduncle is mediolaterally thickened, like that of *E. caroljonesa* (McDonald et al., 2012a), but lacks the projecting pubic peduncle evident in *Z. huangi* (Wang et al., 2017).

The iliac contribution to the acetabulum is shallowly concave in lateral view, similar to *E. caroljonesa* (McDonald et al., 2012a), but unlike the deeper acetabular excavations in *B. johnsoni* and *E. regalis* (Godefroit et al., 1998; Campione, 2014). An anteroposteriorly elongate postacetabular ridge extends across the central plate from above the ischial peduncle to below the supraacetabular process, and is of equivalent in size to those of *I. bernissartensis* and *B. johnsoni* (Norman, 1980; Godefroit et al., 1998); however, it lacks the prominent lateral overhang occurring in *Gilmoreosaurus mongoliensis*, *Gobihadros mongoliensis*, and hadrosaurids (Brett-Surman and Wagner, 2007; Prieto-Márquez and Norell, 2010; Tsogtbaatar et al., 2019).

The postacetabular process of PMU 24720/17 is incomplete but was probably longer than those of *B. johnsoni*, *E. caroljonesa*, and *Z. huangi* (Godefroit et al., 1998; McDonald et al., 2012a; Wang et al., 2017), and alternatively approached the proportions of the postacetabular processes seen in *I. bernissartensis* and *E. regalis* (Norman, 1980; Campione, 2014). Note, though, that postacetabular process length varies considerably in *E. caroljonesa* (McDonald et al., 2017) and *Iguanodon galvensis* Verdú, Royo-Torres, Cobos, and Alcalá, 2015 (Verdú et al., 2017). Additionally, the straight dorsal and ventral surfaces of the postacetabular processes in PMU 24720/17 resemble those of *I. bernissartensis* and *B. johnsoni* (Norman, 1980; McDonald et al., 2012a), suggesting a symmetrical lateral profile that contrasts with the asymmetrical postacetabular processes otherwise typical of most hadrosaurids (Campione, 2014; Prieto-Márquez and Joshi, 2015).

Femur—The right femur, PMU 24720/27 (Fig. 10A–E), is slightly posteriorly bowed. Its proximal end was diagenetically compacted but the femoral head was clearly medially directed. The anterior trochanter is reduced and situated anterior to the greater trochanter, which has a more pronounced dorsal extension. A proximodistal groove separates the anterior and greater trochanters. The fourth trochanter was reconstructed in plaster but is mediolaterally flattened and posteriorly projecting. Attachment scars for the m. puboischiofemoralis internus and m. caudofemoralis longus border the fourth trochanter anteromedially (see Campione, 2014). The insertion for the m. caudofemoralis longus is delimited by a proximodistal ridge that borders a rugose area for the m. puboischiofemoralis internus (Campione, 2014).

The distal end of the femur is divided into lateral and medial condyles, which are anteroposteriorly expanded and approximately equivalent in size. These fully enclose the extensor tunnel anteriorly, as in other hadrosauroids (e.g., *Hadrosaurus foulkii* Leidy, 1858; Prieto-Márquez et al., 2006); however, the posterior flexor tunnel is also fully enclosed, which is a unique condition of *Tanius sinensis*.

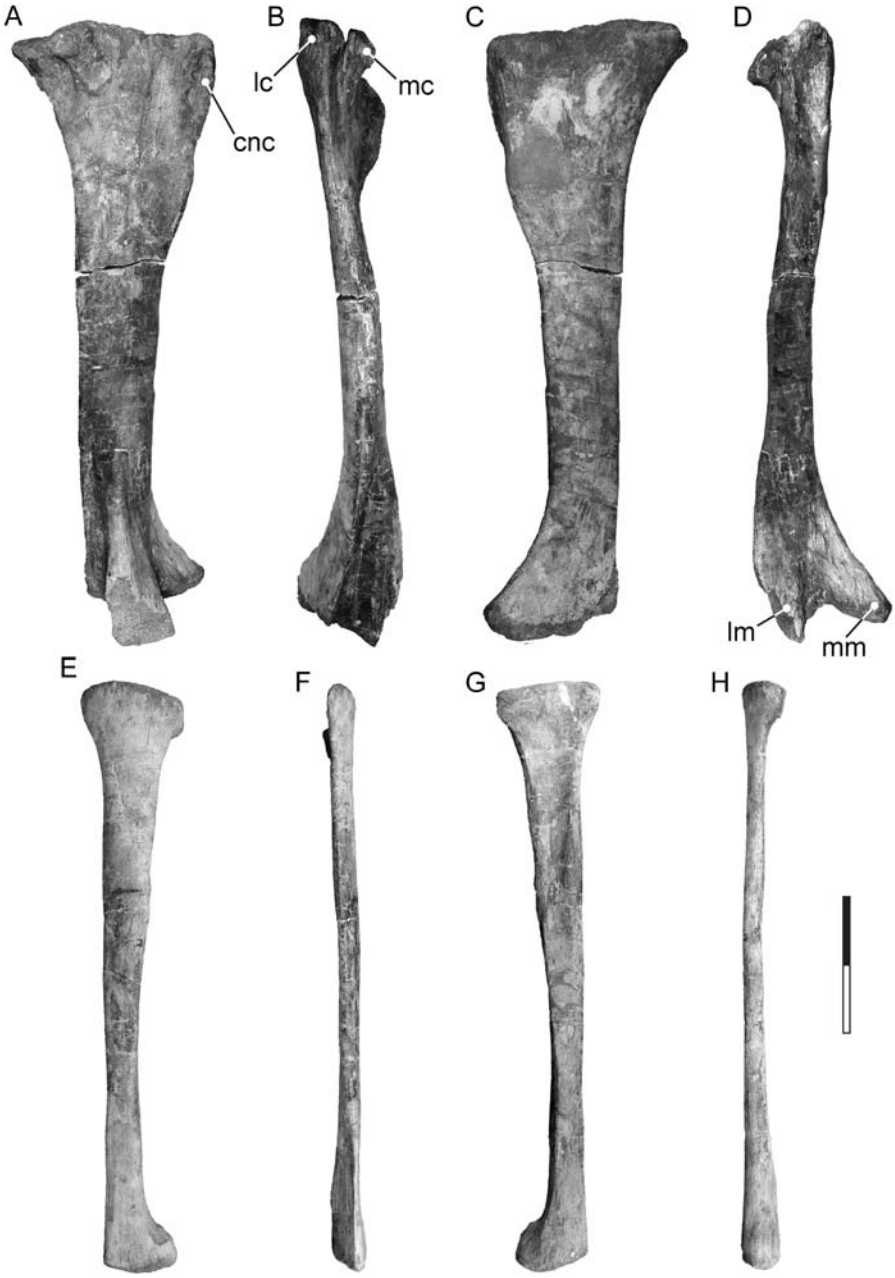

FIGURE 11. *Tanius sinensis* holotype hind limb elements. Right tibia (PMU 24720/28) in **A**, lateral, **B**, anterior, **C**, medial, and **D**, posterior view. Right fibula (PMU 24720/29) in **E**, lateral, **F**, posterior, **G**, medial, and **H**, anterior view. Scale bar equals 200 mm. **Abbreviations**: **cnc**, cnemial crest; **lc**, lateral condyle; **mc**, medial condyle; **lm**, lateral malleolus; **mm**, medial malleolus.

Tibia—The right tibia, PMU 24720/28 (Fig. 11A–D), is massive with perpendicularly offset proximal and distal articular surfaces. The proximal articular surface is anteroposteriorly expanded like those of *Iguanodon bernissartensis*, *Bactrosaurus johnsoni*, and *Eolambia caroljonesa* (Norman, 1980; Godefroit et al., 1998; McDonald et al., 2012a). The cnemial crest is laterally demarcated by a broad depression that extends along the proximal half of the shaft, as in many hadrosauroids (Godefroit et al., 1998). A deep cleft separates the medial and lateral condyles, whose combined width is broader than those of *B. johnsoni*, *E. caroljonesa*, and *Edmontosaurus regalis* (Godefroit et al., 1998; McDonald et al., 2012a; Campione, 2014).

The shaft of the tibia is mediolaterally flattened in cross-section, and the distal articular surface is sub-divided into lateral and medial malleoli separated by a deep groove.

Fibula—The right fibula, PMU 24720/29 (Fig. 11E–H), is slender and straight. A medial trough extends along the proximal third of the shaft, which is shorter than that documented in *Edmontosaurus regalis* where the medial trough continues until about the mid-length of the bone (Campione, 2014). The fibular shaft gradually tapers distally but expands again into a 'club-like' distal end. The distal articular extremity is 'teardrop-shaped' in outline and longest along is anteroposterior axis.

Metatarsals—Wiman (1929) initially interpreted the left metatarsal III, PMU 24720/31 (Fig. 12A–C) as a metatarsal IV, but the element has a longer and straighter profile and thus more closely resembles the metatarsal III morphology of hadrosaurids (Horner et al., 2004). This interpretation is further supported by the conspicuously elongate proximal end and symmetrical distal end (Zheng et al., 2011; McDonald et al., 2012a; Campione,

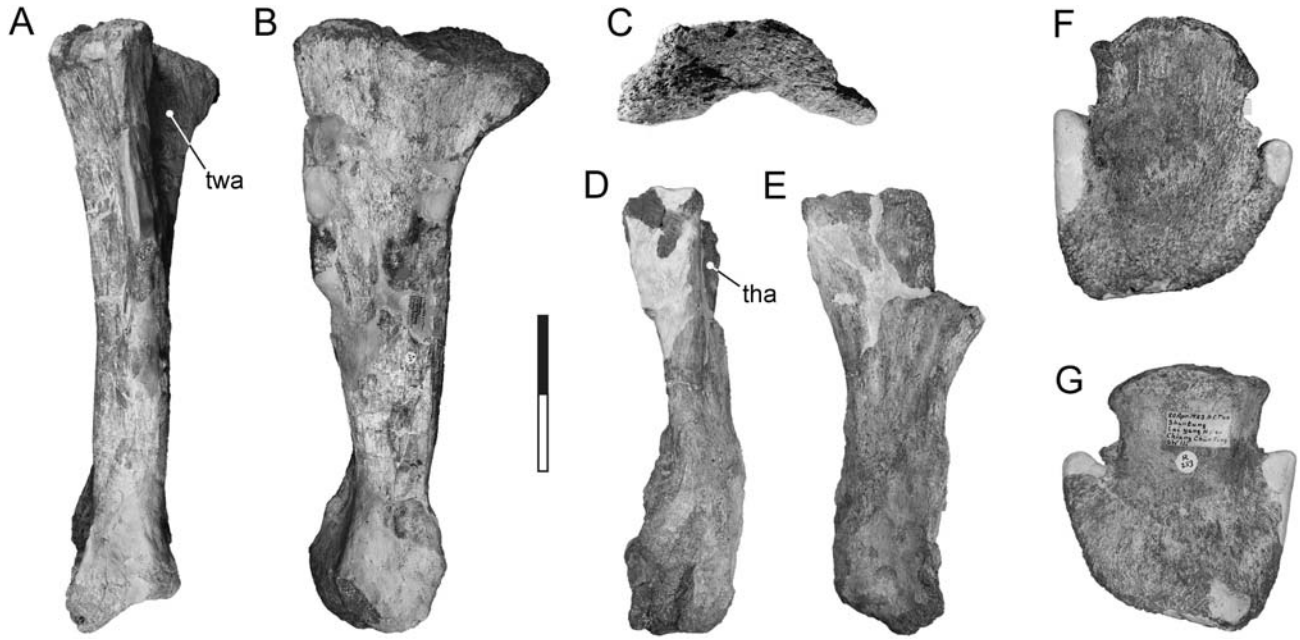

FIGURE 12. *Tanius sinensis* holotype pedal elements. Left metatarsal III (PMU 24720/31) in **A**, posterior, **B**, medial, and **C**, proximal view. Right metatarsal II (PMU 24720/30) in **D**, posterior and **E**, medial view. Right pedal ungual phalanx (PMU 24720/32) in **F**, dorsal and **G**, ventral view. Scale bar equals 100 mm for **A**–**E**; 50 mm for **F**, **G**. **Abbreviations**: **tha**, metatarsal III articulation; **twa**, metatarsal II articulation.

2014). Despite having suffered superficial erosion and mediolateral compression during diagenesis, the proximal end of PMU 24720/31 is distinctly lunate in shape, as in *Secernosaurus koerneri* Brett-Surman, 1979 and *Magnapaulia laticaudus* (Prieto-Márquez and Salinas, 2010; Prieto-Márquez et al. 2012). This differs from the more triangular proximal profiles on the metatarsals of *Bactrosaurus johnsoni*, *Probactrosaurus gobiensis* and *Mantellisaurus atherfieldensis* (Hooley, 1925) (Norman, 1986; Godefroit et al., 1998; Norman, 2002; Paul, 2008), or the rectangular shape of *Lophorothon atopus* Langston, 1960 (Gates and Lamb 2021), D-shaped outline in *Gilmoreosaurus mongoliensis* (Prieto-Márquez and Norell, 2010), or the lenticular outlines otherwise typical of hadrosaurids (Zheng et al., 2011).

The proximomedial surface of PMU 24720/31 is shallowly concave to accommodate metatarsal II; a corresponding trough on the distolateral surface represents the contact for metatarsal IV. The distal articulation is rugose and noticeably less robust than those of *B. johnsoni* and *Gi. mongoliensis* (Godefroit et al., 1998; Prieto-Márquez and Norell, 2010), but is similar to that of *Nanyangosaurus zhugeii* (Xu et al., 2000).

Wiman (1929) did not describe the right metatarsal II, PMU 24720/30 (Fig. 12D, E), which is poorly preserved and partly reconstructed in plaster. Nonetheless, the bone is mediolaterally compressed like the metatarsals of other hadrosauroids (Horner et al., 2004). The medial surface of the shaft is smooth, but the lateral surface is rugose for contact with metatarsal III. The exposed distal extremity is 'squared-off' with a shallow posterior trough that creates an irregular triangular outline.

Pedal Ungual—The pedal ungual phalanx, PMU 24720/31 (Fig. 12F, G), probably derives from the right digit II based on its asymmetrical shape and overall proportions (Godefroit et al., 1998; Zheng et al., 2011). The ungual process is 'hoof-like', similar to those of *Bactrosaurus johnsoni*, but more elongate in dorsal view (Godefroit et al., 1998; McDonald et al., 2012a) and lacking the tapered shape seen in *Gilmoreosaurus mongoliensis* (Prieto-Márquez and Norell, 2010). The dorsal surface of the ungual process in PMU 24720/31 is convex, while the ventral surface is concave. The tip of the ungual process is rugose but has been damaged by weathering. The proximal articulation is concave and oval in outline.

Pathological Bone Modifications

The caudal vertebra PMU 24720/12 bears three conspicuous and closely arranged pits on its left lateral surface (Supplemental Data 3, Fig. S1A, B). These show evidence of peripheral bone fiber remodeling consistent with callus formation and healing after a puncture injury (based on the pathological bone modification categories listed by Pardo-Pérez et al., 2018). The dorsal-most of these traces is situated close to the neurocentral suture and was deep enough to penetrate into the spongiosa. The immediately adjacent trace is drawn out into an elliptical gouge. We interpret these bone modifications as probable bite marks that compare with similar pathologies reported on hadrosauroid caudal vertebrae found elsewhere (e.g., Carpenter, 2000; Canudo et al., 2005; Rivera-Sylva et al., 2009; DePalma et al., 2013; Murphy et al., 2013). The only currently identified terrestrial carnivores from the Jiangjunding Formation faunal assemblage that would have been large enough to inflict such bite traumas are tyrannosauroid theropods. Tyrannosauroid remains were recovered in association with PMU 24720 and occur throughout other strata in the Wangshi Group succession (e.g., Hone et al., 2011; Brusatte et al., 2013; Poropat and Kear, 2013b).

Estimated Body Mass of PMU 24720

We calculated an average body mass range for the PMU 24720 holotype individual of *Tanius sinensis* at between 2091 kg and 3533 kg based on its humeral and femoral circumferences and the scaling equation presented in Campione and Evans (2012). This estimate includes an associated % prediction error and spans the mass ranges typical for hadrosaurids, including *Prosaurolophus maximus* Brown, 1916 (2315–3910 kg), *Lambeosaurus lambei* Parks, 1923 (2454–4146 kg), and *Corythosaurus casuarius*

Brown, 1914 (2570–4341 kg). *Tanius sinensis* also appears to have been larger, on average, than other non-hadrosaurid hadrosauroids, such as *Bactrosaurus johnsoni* (1337–2258 kg) and *Gilmoreosaurus mongoliensis* (966–1631 kg) using the limb circumference data from Benson et al. (2014). We emphasize that *T. sinensis* was significantly smaller than the coeval *Shantungosaurus giganteus*, which reached masses of between 12,918 kg and 21,822 kg, and presumably occupied a very different ecological niche (Benson et al., 2014; Hone et al., 2014).

Other Skeletal Remains

Dorsal Rib—Wiman (1929) attributed a dorsal rib, PMU 22481 (Supplemental Data 3, Fig. S2A), to the *Tanius sinensis* hypodigm. This element is virtually complete, and includes the capitulum, tuberculum, and an entire shaft that lacks only its distalmost extremity. Comparisons with the articulated skeletons of *Edmontosaurus regalis* (Campione, 2014) suggest that PMU 22481 probably derived from the anterior to mid-dorsal region of the axial skeleton, based on the overall length of the rib and the ventrally deflected capitulum relative to the shaft.

The rib head on PMU 22481 has a dorsoventrally broad capitulum, which is acutely offset relative to the shaft. The tuberculum is 'teardrop-shaped' in articular aspect, and thus resembles those on the dorsal ribs of *E. regalis* (Campione, 2014), but differs from the more elliptical tubercula in *Bactrosaurus johnsoni* (Godefroit et al., 1998). The rib shaft of PMU 22481 is mediolaterally flattened.

Humerus—The referred left humerus, PMU 24721 (Supplemental Data 3, Fig. S2B, C) closely resembles the holotype specimen PMU 24720/22, although it is stouter and more medially bowed with an angular distal extremity on the deltopectoral crest. The humeral head of PMU 24721 is also slightly lunate in proximal view, which is similar to that of *Edmontosaurus regalis* (Campione, 2014), but distinguished from the distinctly rounded humeral head of *Eolambia caroljonesa* (McDonald et al., 2012a). In addition, the proximal articular surface on the humeral head of PMU 24721 is bordered by pronounced lateral and medial ledges and has less distinct muscle scarring for the m. latissimus dorsi. Distally, the radial and ulnar condyles of PMU 24721 are separated by an intercondylar groove, although this is demonstrably shorter than that of PMU 24720/22.

Radius—The referred radius, PMU 22483 (Supplemental Data 3, Fig. S2D–G), is closely compatible with the holotype specimens PMU 24720/25–26. Its slender shaft is transversely compressed and expands towards the proximal and distal articular ends. The shaft is also gently curved, like the radii of *Bactrosaurus johnsoni* and *Eolambia caroljonesa* (Godefroit et al., 1998; McDonald et al., 2012a). The proximal articular extremity of PMU 22483 is 'leaf-shaped' in outline, while the distal extremity is quadrangular.

Metatarsal—The referred metatarsal, PMU 22482 (Supplemental Data 3, Fig. S2H, I), has not been fully prepared. However, it appears to be straight and has a prominent 'teardrop-shaped' depression on the medial side of the distal articular surface. The anteroposterior width of the bone indicates that it is probably a metatarsal II based on comparisons with other hadrosauroids (see Zheng et al., 2011).

DISCUSSION

Comparison of Postcranial Character States

The recovered vertebrae of *Tanius sinensis* are morphologically consistent with those of other hadrosauroids, and in particular the cervicals, which are opisthocoelous and possess elongate, dorsally arched postzygapophyses (Norman, 2004; Horner et al., 2004; McDonald et al., 2012a; Campione, 2014). The unusually high neural spine to centrum height ratio (=3.2) on the dorsal vertebra of *T. sinensis* is also reminiscent of derived lambeosaurine hadrosaurids, as well as some iguanodontians, such as *Ouranosaurus nigeriensis* (Taquet, 1976; Prieto-Márquez, 2011b).

The convex dorsal edge on the scapula of *T. sinensis* is consistent with the synapomorphic condition advocated for Hadrosauridae by Prieto-Márquez (2010a). Nevertheless, this may vary ontogenetically (Prieto-Márquez, 2014; Guenther, 2014; Verdú et al., 2017) and is seemingly homoplastic given that similar scapular profiles have been identified in other non-hadrosaurid hadrosauroids, including *Telmatosaurus transylvanicus*, *Tethyshadros insularis*, *Gilmoreosaurus mongoliensis*, *Claosaurus agilis* Marsh, 1872, and *Zhanghenglong yangchengensis* (Dalla Vecchia, 2006; 2009; Prieto-Márquez and Norrell, 2010; Prieto-Márquez, 2011a, 2011c; Xing et al., 2014b).

Prieto-Márquez (2011a) likewise reported that the deltoid ridge on the scapula of *Bactrosaurus johnsoni* becomes more robust and elongate with osteological maturity. Relative ossification must also have affected the proximal articular surface, which is dorsoventrally expanded relative to the distal end of the scapula in *T. sinensis*, and resembles other non-hadrosaurid hadrosauroids (Prieto-Márquez and Norell, 2010). Unusually, however, the anterodorsally curved acromion process in *T. sinensis* is equivalent to the derived condition characterizing lambeosaurines, but may be homoplastic given its occurrence elsewhere in iguanodontians (e.g., *Iguanodon bernissartensis*) and other non-hadrosaurid hadrosauroids, such as *Eolambia caroljonesa* (Prieto-Márquez, 2010a).

The ilia of *T. sinensis* exhibit anteroventrally projecting preacetabular processes that are typical of hadrosauroids (Horner et al., 2004; Prieto-Márquez, 2010a). Orientation of the preacetabular process at ~145° (which is less than the value obtained by Prieto-Márquez, 2010b) is also common among ornithopods but may vary intraspecifically in hadrosauroids (Brett-Surman and Wagner, 2007; Prieto-Márquez, 2010a; Campione, 2014; Verdú et al., 2017).

The pubic peduncle of *T. sinensis* is reduced relative to the ischial peduncle, and the central plate of the ilium is almost symmetrical with a depth/length ratio of 0.91; this is a plesiomorphic condition among hadrosauroids (Prieto-Márquez, 2010a). Similarly, positioning of the ventral apex of the supraacetabular process posterodorsal to the ischial peduncle approaches the placement in *I. bernissartensis*, as well as other non-hadrosaurid hadrosauroids (Prieto-Márquez and Norell, 2010). Lastly, reduction of the supraacetabular process to a narrow shelf in *T. sinensis* (limiting its lateroventral projection: sensu Prieto-Márquez, 2010a), together with a straight dorsal ilial profile are typical in hadrosauroids (Prieto-Márquez, 2007; Campione, 2014).

The weakly projecting postacetabular ridge above the ischial peduncle of *T. sinensis* is compatible with the apomorphic trait interpreted for hadrosaurids, and is notably absent in iguanodontians (Brett-Surman, 1977; Godefroit et al., 1998). However, several non-hadrosaurid hadrosauroids have since been found to possess postacetabular ridges, including *Gi. mongoliensis*, *Huehuecanauhtlus tiquichensis* Ramírez-Velasco, Benammi, Prieto-Márquez, Ortega, and Hernández-Rivera 2012, and *Zuoyunlong huangi* (Gilmore, 1933; Ramírez-Velasco et al., 2012; Wang et al., 2017), as well as possibly *Bolong yixianensis* Wu, Godefroit and Hu, 2010 (Wu et al., 2010).

The straight femoral shaft of *T. sinensis* conforms to the derived state among hadrosaurids (Prieto-Márquez, 2010a; McDonald et al., 2012b; Xing et al., 2014a); however, Verdú et al. (2017) also demonstrated intraspecific variability in *I. bernissartensis*. Alternatively, the posterior fusion of the medial and lateral distal condyles to form an enclosed flexor tunnel constitutes a unique character state for *T. sinensis*, which was also noticed by Wiman (1929:55), who described it as "Zwischen den beiden Condyli liegen zwei Löcher" (literally

translated to "between the two condyli, two holes are situated"). Although perhaps ontogenetically related (Grigorescu and Csiki, 2006), a fully enclosed flexor tunnel contrasts with the usual hadrosaurid condition of having only the anterior extremities of the lateral and medial femoral condyles fused together (Horner et al., 2004; Juárez Valieri et al., 2010); this condition is also present in *T. transylvanicus* (Weishampel et al., 1993), *B. johnsoni* (Godefroit et al., 1998), *Gobihadros mongoliensis* (Tsogtbaatar et al., 2019), and the iguanodontians *O. nigerensis* (Taquet, 1976) and *Proa valdearinnoensis* McDonald, Espílez, Mampel, Kirkland and Alcalá, 2012b (McDonald et al., 2012b). Importantly, posterior elongation of the flexor tunnel occurs in *Tsintaosaurus spinorhinus* and *Shantungosaurus giganteus* (Young, 1958; Hu et al., 2001), but this can be discriminated from the autapomorphically complete enclosure found in *T. sinensis*.

Although influenced by ontogeny (Brett-Surman and Wagner, 2007), ventral extension of the cnemial crest onto the proximal half of the tibia shaft in *T. sinensis* is shared with *T. transylvanicus*, *Gi. mongoliensis*, *B. johnsoni*, *Nanyangosaurus zhugeii*, *Nanningosaurus dashiensis*, *Yunganglong datongensis* Wang, You, Xu, Wang, Yi, Xie, Jia, and Li, 2013, and *Go. mongoliensis*, as well as hadrosaurids (Weishampel et al., 1993; Godefroit et al., 1998; Xu et al., 2000; Mo et al., 2007; Prieto-Márquez and Norell, 2010; Wang et al., 2013; Tsogtbaatar et al., 2019). Likewise, expansion of the distal end of the fibula is intraspecifically variable (Brett-Surman and Wagner, 2007), but resembles the condition in lambeosaurines (Prieto-Márquez, 2010a).

In the pes, the slender metatarsal III of *T. sinensis* has a length/width ratio of >4.5, which reflects the derived state among hadrosauroids (Prieto-Márquez, 2010a). Similarly, the hoof-like pedal ungual, while also typical of hadrosauroids (Norman, 2004), lacks the proximodistally short and broad dorsal outline characteristic of hadrosaurids (Horner et al., 2004; Prieto-Márquez, 2010a). The lateral grooves on the pedal ungual of *T. sinensis* also compare with non-hadrosaurid hadrosauroids, such as *T. insularis*, *N. zhugeii*, and *Protohadros byrdi* Head, 1998 (McDonald et al., 2012a).

Taxonomic Implications

Although sometimes considered ambiguously diagnostic (e.g., Weishampel and Horner, 1990), the taxonomic validity of the *Tanius sinensis* type material (PMU 24720/1–32) has never been questioned, and, indeed, is reinforced by our identification of multiple potential autapomorphies in the postcranial skeleton. Unfortunately, however, the other proposed species of *Tanius*—*Tanius chingkankouensis* and *Tanius laiyangensis*—were established on postcranial remains from Upper Cretaceous (probable upper Campanian) strata of the Jingangkou Formation (Young, 1958; Zhen, 1976) that have questionable character state utility.

Tanius chingkankouensis—Young (1958) erected this species on the basis of an aggregated series of cervical and dorsal vertebrae, a sacrum, scapula, ilium, and ischium. Young (1958) referred this material to the genus *Tanius* because of overall similarity with the cervical vertebrae of PMU 24720. Young (1958) further designated these remains as the composite holotype of a separate species because the posterior sacral vertebrae bore a furrow along their ventral surfaces. Subsequent studies have, nevertheless, shown this particular state to be broadly distributed throughout Hadrosauroidea (Godefroit et al., 1998; Norman, 1998; Horner et al., 2004; Prieto-Márquez, 2008), and possibly also intraspecifically variable (Hone et al., 2014). The widespread occurrence of a ventral furrow on the cervical vertebrae was also acknowledged by Zhang et al. (2017), who reaffirmed affinity between *T. chingkankouensis* and PMU 24720 based on their shared possession of parallel dorsal and ventral margins on the distal scapular blade. Zhang et al. (2017) additionally argued that *T. chingkankouensis* must be valid because its scapular blade is straight, as opposed to the distinctively curved dorsal margin on the scapula of PMU 24720/20. Yet from our observations, PMU 24720/20 differs markedly in its narrower distal end on the scapular blade, strongly curved acromion process, and relatively more robust glenoid. The potential for intraspecific variability should also be considered since it affects the scapular blade in other iguanodontians (Guenther, 2009, 2014; Verdú et al. 2017). Moreover, Zhang et al. (2017:195, 196) concluded that the ilium associated with *T. chingkankouensis* could not be referred to *Tanius* because the "apex of the supraacetabular process is located anterodorsal to the caudal tuberosity of the ischial peduncle", which is "a characteristic of saurolophines (Prieto-Márquez, 2008, 2010[b])". While we agree with this conclusion, we also point out that the PMU 24720/18 ilium differs in its straighter dorsal margin and more prominent supraacetabular processes.

Weishampel and Horner (1990), Buffetaut and Tong-Buffetaut (1993), and Buffetaut (1995) all initially considered the *T. chingkankouensis* composite material to be an invalid taxon, which has since been regarded as either a junior synonym of *Tanius sinensis* (Horner et al., 2004; Lund and Gates, 2006), or a nomen dubium (Prieto-Márquez and Wagner, 2013). However, given that Zhang et al. (2017) excluded the ilium, and, as we show, generic referral of the scapula to *Tanius* is problematic, we deem a general similarity of the cervicals to be insufficient grounds for unambiguously asserting a taxonomic relationship. In our opinion, therefore, *T. chingkankouensis* should be regarded as a nomen dubium (sensu Prieto-Márquez and Wagner, 2013) that incorporates hadrosaurid skeletal elements (sensu Zhang et al., 2020), together with an ischium that "has a slightly inflated distal end" "characteristic of basal hadrosauroids (Prieto-Márquez, 2008, 2010[b])" Zhang et al. (2017:196), and also probably various other non-hadrosaurid hadrosauroid bones.

Tanius laiyangensis—Zhen (1976) named *T. laiyangensis* from a sacrum and right ilium, which Zhang et al. (2020) recently interpreted as representing a single individual. Zhen (1976) did not provide specific locality information for these remains, but Zhang et al. (2020) confirmed their recovery from the same horizon as the composite material of *T. chingkankouensis*. *Tanius laiyangensis* was distinguished by a combination of features, including: "taller neural spines, more robust sacral bars, elongate ventral sulcus and horizontally oriented transverse processes of the sacrum, and the proportionally longer postacetabular process of the ilium" (see Zhang et al., 2020:793). Conversely, a detailed re-examination of *T. laiyangensis* by Zhang et al. (2020) concluded that all these features were consistent with advanced hadrosaurids, and thus proposed reassignment as an indeterminate kritosaurin. This concurs with previous assertions that *T. laiyangensis* is incompatible with *Tanius* (Weishampel and Horner, 1990; Buffetaut, 1995; Horner et al., 2004; Zhang et al., 2017), and supports our own observations that PMU 24720/18 can be distinguished from the *T. laiyangensis* remains by its shorter and deeper iliac profile, more prominent supraacetabular process, shallower embayment between the preacetabular ridge and pubic peduncle, and relatively more ventrally deflected preacetabular process. In any case, we agree with Zhang et al. (2020) that *T. laiyangensis* is an invalid taxon erected on indeterminate hadrosaurid material.

Bactrosaurus prynadai—Although not described as a species of *Tanius*, *B. prynadai* was established by Riabinin (1939) from a partial maxilla and associated dentaries found in Upper Cretaceous (Coniacian–Santonian) deposits of the Kyrk-Kuduk region in southern Kazakhstan. Confusingly, Young (1958) decided that sufficient similarities existed to warrant transfer of this species to *Tanius* after examining a skull (AMNH 6365) previously referred

to *Bactrosaurus johnsoni* by Gilmore (1933). Maryańska and Osmólska (1981) followed this conclusion with a tentative referral of AMNH 6365 to *Tanius* sp. but regarded *B. prynadai* as a nomen dubium without explanation. Alternatively, Rozhdestvensky (1966:112) stated that "[t]he species [of *Bactrosaurus*] described from the south of Kazakhstan refers, probably, to the genus *Yaxartosaurus*[sic]" [translated from Russian], and later clarified this hypothesis (Rozhdestvensky, 1967:563) by mentioning that "*Bactrosaurus prynadai*, described by R[i]abinin (1939), is probably a young individual of *Jaxartosaurus aralensis* R[i]abinin, 1939, with which it was found" (see also Rozhdestvensky, 1968). However, this synonymy has received little support, and *Bactrosaurus prynadai* is usually classified as a nomen dubium (Weishampel and Horner, 1990; Norman and Sues, 2000; Horner et al., 2004; Lund and Gates, 2006). Furthermore, AMNH 6365 was attributed to *Gilmoreosaurus mongoliensis* by Weishampel and Horner (1986) but has elsewhere been retained within *B. johnsoni* (Godefroit et al., 1998; Prieto-Márquez and Norell, 2010; Prieto-Márquez, 2011a).

***Tsintaosaurus spinorhinus*—**Rozhdestvensky (1964) considered *Tsintaosaurus spinorhinus* to be a junior synonym of *Tanius sinensis*, suggesting that the missing rostral section of the skull in PMU 24720/1a might have supported a crest. Rozhdestvensky (1974, 1977) subsequently revised this interpretation, claiming that *T. spinorhinus* and *T. sinensis* could be congeneric but not conspecific. Weishampel and Horner (1990) further argued that *T. spinorhinus* was based on composite lambeosaurine and hadrosaurine remains, and that its famous spike-like crest was a displaced nasal. This reinterpretation was justified via a personal communication that was later elaborated by Taquet (1991), who proposed that *T. spinorhinus* was probably a crestless hadrosauroid and a junior synonym of *Tanius sinensis*. Buffetaut and Tong-Buffetaut (1993) refuted this suggestion, citing key differences in cranial osteology. Prieto-Márquez and Wagner (2013) and Zhang et al. (2017) also both conclusively demonstrated that a cranial crest was present in *T. spinorhinus*, as well as the lack of a comparable structure in *T. sinensis* (see Zhang et al., 2017:196, fig. 4A), a conclusion that we reaffirm from our first-hand inspections of PMU 24720.

CONCLUSIONS

Here, we undertake a detailed re-description of the diagnostic holotype postcranial skeleton (PMU 24720/2–32) and other referred elements (PMU 22481, PMU 22482, PMU 22483, PMU 24721) of one of the first dinosaur taxa identified from China—*Tanius sinensis*. These remains constitute some of the many historically important dinosaur fossils recovered by the Sino-Swedish expeditions of the 1920s, and also form part of an ongoing project to restore and re-evaluate the significant collections of this material held in perpetuity at the PMU in Sweden (Poropat, 2013; Poropat and Kear, 2013a, 2013b; Borinder et al. 2016).

Based on our firsthand examination of these remains we identify a unique postcranial character state combination that defines *T. sinensis* among recognized hadrosauroid taxa. These include a scapula with strongly curved dorsal margin, recurved and anterodorsally directed anterior end on the acromion process, and dorsoventrally expanded proximal versus distal extremity, a reduced deltopectoral crest on the humerus, a deep central plate on the ilium, a 'club-like' distal end on the fibula, and a proximodistally elongate metatarsal III. In addition, at least four postcranial apomorphies serve to establish *T. sinensis* as a distinct non-hadrosaurid hadrosauroid species: (1) the presence of a tall neural spine on the dorsal vertebra that equals up to three times the height of the corresponding centrum; (2) a reduced postacetabular ridge on the ilium; (3) uniquely complete fusion of the medial and lateral condyles on the femur to form a fully enclosed flexor tunnel; and (4) a lunate profile on the proximal articular surface of metatarsal III. Furthermore, we report a series of associated pathological bone modifications consistent with healed bite traces found on the holotype caudal vertebra (PMU 24720/12), which might evince an encounter with a predatory tyrannosauroid.

The stylopodial limb circumferences of the *T. sinensis* holotype individual suggest an average body mass of between 2091 kg and 3533 kg, which places this species among the largest non-hadrosaurid hadrosauroids (see Benson et al., 2014, 2018). Furthermore, our taxonomic assessments indicate that *T. sinensis* is the only unambiguously valid species of the genus *Tanius*, which accords with previous assertions that *Tanius chingkankouensis* and *Tanius laiyangensis* should be considered nomina dubia.

Finally, virtually all of the recent phylogenetic analyses integrating *T. sinensis* (e.g., Sues and Averianov, 2009; Prieto-Márquez and Wagner, 2009; McDonald et al., 2010; Prieto-Márquez, 2010a; McDonald, 2012; Xing et al., 2014a; McDonald et al., 2017; Zhang et al., 2020) advocate its placement as a non-hadrosaurid hadrosauroid, closely related to morphologically comparable taxa, including *Bactrosaurus johnsoni* and *Gilmoreosaurus mongoliensis* (e.g., McDonald et al., 2017; Prieto-Márquez, 2010a; Xing et al., 2014a). Nevertheless, *T. sinensis* is stratigraphically younger than all of these other basally branching species, and at late Campanian to early Maastrichtian (Xing et al., 2014b) in age (and at least <72.9–73.5 Ma: Yan et al., 2005), demonstrates that non-hadrosaurid hadrosauroids evidently persisted in both Asia and Europe (e.g., Dalla Vecchia, 2009) long after their hypothesized extinction in Laramidia at around the Santonian–early Campanian interval (Norman, 2004; Evans et al., 2012; Campione et al., 2013).

The recognized fossils of *T. sinensis* are thus of significance for elucidating hadrosauroid diversity and distribution across the Laurasian landmasses towards the end of the Mesozoic. In particular, the faunal context of *T. sinensis* as part of a rich succession of dinosaur assemblage spanning the Jiangjunding and Jingangkou formations (see Zhang et al., 2017) offers the potential to reconstruct ecological segregation between coeval species and will provide a focus for the next of our forthcoming studies on the PMU vertebrate fossil collection from the Wangshi Group of China.

ACKNOWLEDGMENTS

We thank J. O. Ebbestad (Uppsala University) and V. Vajda (Swedish Museum of Natural History) for supporting this study. P. Eriksson (Uppsala University) prepared fossils for our research. Xing H. (Beijing Museum of Natural History), L. Alcalá (Fundación Conjunto Palaeontológico de Teruel-Dinópolis/Museo Aragonés de Palaeontología), and A. Prieto-Márquez (Universitat Autònoma de Barcelona) provided information and data. A. T. McDonald (Western Science Center) and a second anonymous reviewer contributed constructive comments. This work is developed from a Master thesis by NHB that was undertaken at the Department of Earth Sciences at Uppsala University, and was supervised by NEC with examination by J. Hendericks (Uppsala University).

ORCID

Stephen F. Poropat http://orcid.org/0000-0002-4909-1666
Nicolás E. Campione http://orcid.org/0000-0002-4205-9794
Benjamin P. Kear http://orcid.org/0000-0002-3128-3141

LITERATURE CITED

Benson, R. B. J., N. E. Campione, M. T. Carrano, P. D. Mannion, C. Sullivan, P. Upchurch, and D. C. Evans. 2014. Rates of dinosaur

body mass evolution indicate 170 million years of sustained ecological innovation on the avian stem lineage. PLoS Biology 12: e1001853.
Benson, R. B. J., G. Hunt, M. T. Carrano, and N. Campione. 2018. Cope's rule and the adaptive landscape of dinosaur body size evolution. Palaeontology 61:13–48.
Borinder, N. H., S. F. Poropat, and B. P. Kear. 2016. Reassessment of the earliest documented stegosaurian fossils from Asia. Cretaceous Research 68:61–69.
Boulenger, G. A. 1881. Sur l'arc pelvien chez les Dinosauriens de Bernissart. Bulletins de l'Académie royale des sciences, des lettres et des beaux-arts de Belgique 1 (series 3):600–608.
Brett-Surman, M. K. 1977. The appendicular anatomy of hadrosaurian dinosaurs, Vol. Master of Arts, pp. 70. University of California, Berkeley, California.
Brett-Surman, M. K. 1979. Phylogeny and palaeobiogeography of hadrosaurian dinosaurs. Nature 277:560–562.
Brett-Surman, M. K., and J. R. Wagner. 2007. Discussion of character analysis of the appendicular anatomy in Campanian and Maastrichtian North American hadrosaurids - variation and ontogeny; pp. 135–169 in K. Carpenter (ed.), Horns and Beaks: Ceratopsian and Ornithopod Dinosaurs. Indiana University Press, Bloomington & Indianapolis, Indiana.
Brown, B. 1913. A new trachodont dinosaur, *Hypacrosaurus*, from the Edmonton Cretaceous of Alberta. Bulletin of the American Museum of Natural History 32:395–406.
Brown, B. 1914. *Corythosaurus casuarius*, a new crested dinosaur from the Belly River Cretaceous, with provisional classification of the family Trachodontidae. Bulletin of the American Museum of Natural History 33:559–565.
Brown, B. 1916. A new crested trachodont dinosaur, *Prosaurolophus maximus*. Bulletin of the American Museum of Natural History 35:701–708.
Brownstein, C.D. 2020. Osteology and phylogeny of small-bodied hadrosauromorphs from an end-Cretaceous marine assemblage. Zoological Journal of the Linnean Society DOI:10.1093/zoolinnean/zlaa085
Brusatte, S. L., D. W. E. Hone, and X. Xu. 2013. Phylogenetic revision of *Chingkankousaurus fragilis*, a forgotten tyrannosauroid specimen from the Late Cretaceous of China; pp. 2–13 in J. M. Parrish, R. E. Molnar, P. J. Currie, and E. B. Koppelhus (eds.), Tyrannosaurid Paleobiology. Indiana University Press, Bloomington & Indianapolis, Indiana.
Buffetaut, E. 1995. An ankylosaurid dinosaur from the Upper Cretaceous of Shandong (China). Geological Magazine 132:683–692.
Buffetaut, E., and H. Tong-Buffetaut. 1993. *Tsintaosaurus spinorhinus* Young and *Tanius sinensis* Wiman: a preliminary comparative study of two hadrosaurs (Dinosauria) from the Upper Cretaceous of China. Comptes Rendus de l'Académie des Sciences. Série II: Mécanique-Physique, Chimie, Sciences de l'Univers, Sciences de la Terre 317:1255–1261.
Campione, N. E. 2014. Postcranial anatomy of *Edmontosaurus regalis* (Hadrosauridae) from the Horseshoe Canyon Formation, Alberta, Canada; pp. 208–244 in D. A. Eberth, and D. C. Evans (eds.), Hadrosaurs. Indiana University Press, Bloomington & Indianapolis, IA.
Campione, N. E., K. S. Brink, E. A. Freedman, C. T. McGarrity, and D. C. Evans. 2013. '*Glishades ericksoni*', an indeterminate juvenile hadrosaurid from the Two Medicine Formation of Montana: implications for hadrosauroid diversity in the latest Cretaceous (Campanian–Maastrichtian) of western North America. Palaeobiodiversity and Palaeoenvironments 93:65–75.
Campione, N. E., and D. C. Evans. 2012. A universal scaling relationship between body mass and proximal limb bone dimensions in quadrupedal terrestrial tetrapods. BMC Biology 10:1–21.
Campione, N. E., D. C. Evans, and R. Cuthbertson. 2007. Anatomy of the atlas-axis complex of hadrosaurid dinosaurs. Journal of Vertebrate Paleontology 27:55A.
Canudo, J. I., P. Cruzado-Caballero, and M. Moreno-Azanza. 2005. Possible theropod predation evidence in hadrosaurid dinosaurs from the Upper Maastrichtian (Upper Cretaceous) of Arén (Huesca, Spain). Kaupia 14:9–13.
Carpenter, K. 2000. Evidence of predatory behavior by carnivorous dinosaurs; pp. 135–144 in B. P. Pérez-Moreno, T. R. Holtz, Jr., J. L. Sanz, and J. J. Moratalla (eds.), Aspects of Theropod Paleobiology; Gaia, 15.
Cope, E. D. 1870. Synopsis of the extinct Batrachia, Reptilia and Aves of North America. Transactions of the American Philosophical Society 14:1–252.
Dalla Vecchia, F. M. 2006. *Telmatosaurus* and the other hadrosaurids of the Cretaceous European Archipelago. An overview. Natura Nascosta 32:1–55.
Dalla Vecchia, F. M. 2009. *Tethyshadros insularis*, a new hadrosauroid dinosaur (Ornithischia) from the Upper Cretaceous of Italy. Journal of Vertebrate Paleontology 29:1100–1116.
DePalma, R. A., II, D. A. Burnham, L. D. Martin, B. M. Rothschild, and P. L. Larson. 2013. Physical evidence of predatory behavior in *Tyrannosaurus rex*. Proceedings of the National Academy of Sciences 110:12560–12564.
Dilkes, D. W. 2001. An ontogenetic perspective on locomotion in the Late Cretaceous dinosaur *Maiasaura peeblesorum* (Ornithischia: Hadrosauridae). Canadian Journal of Earth Sciences 38:1205–1227.
Dollo, L. 1888. Sur la signification du 'trochanter pendant' des dinosauriens. Bulletin Scientifique de la France et de la Belgique 19:215–224.
Egi, N., and D. B. Weishampel. 2002. Morphometric analyses of humeral shapes in hadrosaurids (Ornithopoda, Dinosauria). Senckenbergiana Lethaea 82:43–58.
Evans, D. C., P. M. Barrett, and K. L. Seymour. 2012. Revised identification of a reported *Iguanodon*-grade ornithopod tooth from the Scollard Formation, Alberta, Canada. Cretaceous Research 33:11–14.
Evans, D. C., and R. R. Reisz. 2007. Anatomy and relationships of *Lambeosaurus magnicristatus*, a crested hadrosaurid dinosaur (Ornithischia) from the Dinosaur Park Formation, Alberta. Journal of Vertebrate Paleontology 27:373–393.
Fuentes Vidarte, C., M. Meijide Calvo, F. Meijide Fuentes, and M. Meijide Fuentes. 2016. Un nuevo dinosaurio estiracosterno (Ornithopoda: Ankylopollexia) del Cretácico Inferior de España. Spanish Journal of Palaeontology 31:407–446. [English abstract]
Gasca, J. M., M. Moreno-Azanza, J. I. Ruiz-Omeñaca, and J. I. Canudo. 2015. New material and phylogenetic position of the basal iguanodont dinosaur *Delapparentia turolensis* from the Barremian (Early Cretaceous) of Spain. Journal of Iberian Geology 41:57–70.
Gasulla, J. M., F. Escaso, I. Narváez, F. Ortega, and J. L. Sanz. 2015. A new sail-backed styracosternan (Dinosauria: Ornithopoda) from the Early Cretaceous of Morella, Spain. PLOS One 10:e0144167.
Gates, T. A. and J. P. Lamb. 2021. A redescription of *Lophorhothon atopus* (Ornithopoda: Dinosauria) from the Late Cretaceous of Alabama based on new material. Canadian Journal of Earth Sciences. DOI:10.1139/cjes-2020-0173.
Gilmore, C. W. 1933. On the dinosaurian fauna from the Iren Dabasu Formation. Bulletin of the American Museum of Natural History 67:23–78.
Godefroit, P., Z.-M. Dong, P. Bultynck, H. Li, and L. Feng. 1998. New *Bactrosaurus* (Dinosauria: Hadrosauroidea) material from Iren Dabasu (Inner Mongolia, P.R. China). Bulletin de L'Institut Royal Des Sciences Naturelles de Belgique 68 (supp.):1–70.
Grigorescu D. and Z. Csiki. 2006. Ontogenetic development of *Telmatosaurus transsylvanicus* (Ornithischia: Hadrosauria) from the Maastrichtian of the Haţeg Basin, Romania – evidence from the limb bones. Hantkeniana 5:20–26.
Guenther, M. F. 2009. Influence of sequence heterochrony on hadrosaurid dinosaur postcranial development. The Anatomical Record 292:1427–1441.
Guenther, M. F. 2014. Comparative ontogenies (appendicular skeleton) for three hadrosaurids and a basal iguanodontian: divergent developmental pathways in Hadrosaurinae and Lambeosaurinae; pp. 398–415 in D. A. Eberth, and D. C. Evans (eds.), Hadrosaurs. Indiana University Press, Bloomington & Indianapolis.
Head, J. J., 1998. A new species of basal hadrosaurid (Dinosauria, Ornithopoda) from the Cenomanian of Texas. Journal of Vertebrate Paleontology 18:718–738.
Hone, D. W. E., K. Wang, C. Sullivan, X. Zhao, S. Chen, D. Li, S. Ji, Q. Ji, and X. Xu. 2011. A new, large tyrannosaurine theropod from the Upper Cretaceous of China. Cretaceous Research 32:495–503.
Hone, D. W. E., C. Sullivan, Q. Zhao, K. Wang, and X. Xu. 2014. Body size distribution in a death assemblage of a colossal hadrosaurid from the Upper Cretaceous of Zhucheng, Shandong Province,

China pp. 524–531 in D. A. Eberth, and D. C. Evans (eds.), Hadrosaurs. Indiana University Press, Bloomington & Indianapolis.
Hooley, R.W. 1925. On the skeleton of *Iguanodon atherfieldensis* sp. nov., from the Wealden Shales of Atherfield (Isle of Wight). Quarterly Journal of the Geological Society of London 81:1–61.
Horner, J. R., D. B. Weishampel, and C. A. Forster. 2004. Hadrosauridae; pp. 438–463 in D. B. Weishampel, P. Dodson, and H. Osmólska (eds.), The Dinosauria: Second Edition. University of California Press, Berkeley.
Hu, C.-C. 1973. A new hadrosaur from the Cretaceous of Chucheng, Shantung. Acta Geologica Sinica 2:179–206.
Hu, C., Z. Cheng, Q. Pang, and X. Fang. 2001. *Shantungosaurus giganteus*. 139 pp. Geological Publishing House, Beijing.
Huene, F. v. 1956. Paläontologie und Phylogenie der Niederen Tetrapoden. 716 pp. Gustav Fischer, Jena, Germany.
Juárez Valieri, R. D., J. A. Haro, L. E. Fiorelli, and J. O. Calvo. 2010. A new hadrosauroid (Dinosauria: Ornithopoda) from the Allen Formation (Late Cretaceous) of Patagonia, Argentina. Revista del Museo Argentino de Ciencias Naturales 12:217–231.
Kirkland, J. I. 1998. A new hadrosaurid from the Upper Cedar Mountain Formation (Albian-Cenomanian: Cretaceous) of eastern Utah - the oldest known hadrosaurid (lambeosaurine?); pp. 283–296 in S. G. Lucas, J. I. Kirkland, and J. W. Estep (eds.), Lower and Middle Cretaceous Terrestrial Ecosystems: New Mexico Museum of Natural History and Science Bulletin, 14.
Lambe, L. M. 1914. On *Gryposaurus notabilis*, a new genus and species of trachodont dinosaur from the Belly River Formation of Alberta, with a description of the skull of *Chasmosaurus belli*. Ottawa Naturalist 27:145–155.
Lambe, L. M. 1917. A new genus and species of crestless hadrosaur from the Edmonton Formation of Alberta. Ottawa Naturalist 31:65–73.
Langston W., Jr. 1960. The vertebrate fauna of the Selma Formation of Alabama, part VI: the dinosaurs. Fieldiana: Geology Memoirs 3:315–361.
Leidy, J. 1858. *Hadrosaurus foulkii*, a new saurian from the Cretaceous of New Jersey, related to Iguanodon. Proceedings of the Academy of Natural Sciences of Philadelphia 10:213-218.
Lund, E. K., and T. A. Gates. 2006. A historical and biogeographic examination of hadrosaurian dinosaurs; pp. 263–276 in S. G. Lucas, and R. M. Sullivan (eds.), Late Cretaceous Vertebrates from the Western Interior: New Mexico Museum of Natural History and Science Bulletin 35.
Marsh, O. C. 1872. Notice on a new species of *Hadrosaurus*. American Journal of Science 3:301.
Marsh, O. C. 1881. Principal characters of American Jurassic dinosaurs. Part V. American Journal of Science 21 (series 3):417–423.
Maryańska, T., and H. Osmólska. 1981. Cranial anatomy of *Saurolophus angustirostris* with comments on the Asian Hadrosauridae (Dinosauria); Results of the Polish-Mongolian Palaeontological Expeditions - Part IX. Palaeontologia Polonica 42:5–24.
Maryańska, T., and H. Osmólska. 1984. Postcranial anatomy of *Saurolophus angustirostris* with comments on other hadrosaurs; Results of the Polish-Mongolian Palaeontological Expeditions - Part X. Palaeontologia Polonica 46:119–141.
Mateer, N. J., and J. S. McIntosh. 1985. A new reconstruction of the skull of *Euhelopus zdanskyi* (Saurischia: Sauropoda). Bulletin of the Geological Institutions of the University of Uppsala 11:124–132.
McDonald, A. T. 2012. Phylogeny of basal iguanodonts (Dinosauria: Ornithischia): an update. PLoS One 7:e36745.
McDonald, A. T., J. Bird, J. I. Kirkland, and P. Dodson. 2012a. Osteology of the basal hadrosauroid *Eolambia caroljonesa* (Dinosauria: Ornithopoda) from the Cedar Mountain Formation of Utah. PLoS One 7:e45712.
McDonald, A. T., E. Espílez, L. Mampel, J. I. Kirkland, and L. Alcalá. 2012b. An unusual new basal iguanodont (Dinosauria: Ornithopoda) from the Lower Cretaceous of Teruel, Spain. Zootaxa 3595:61–76.
McDonald, A. T., T. A. Gates, L. E. Zanno, and P. J. Makovicky. 2017. Anatomy, taphonomy, and phylogenetic implications of a new specimen of *Eolambia caroljonesa* (Dinosauria: Ornithopoda) from the Cedar Mountain Formation, Utah, USA. PLoS One 12:e0176896.
McDonald, A. T., J. I. Kirkland, D. D. DeBlieux, S. K. Madsen, J. Cavin, A. R. C. Milner, and L. Panzarin. 2010. New basal iguanodonts from the Cedar Mountain Formation of Utah and the evolution of thumb-spiked dinosaurs. PLoS One 5:e14075.
Mo, J., Z. Zhao, W. Wang, and X. Xu. 2007. The first hadrosaurid dinosaur from southern China. Acta Geologica Sinica 81:550–554.
Morris, W. J. 1981. A new species of hadrosaurian dinosaur from the Upper Cretaceous of Baja California-?*Lambeosaurus laticaudus*. Journal of Paleontology 55:453–462.
Murphy, N. L., K. Carpenter, and D. Trexler. 2013. New evidence for predation by a large tyrannosaurid; pp. 279–286 in J. M. Parrish, R. E. Molnar, P. J. Currie, and E. B. Koppelhus (eds.), Tyrannosaurid Paleobiology. Indiana University Press, Bloomington & Indianapolis, Indiana.
Nopcsa, F. B. 1900. Dinosaurierreste aus Siebenbürgen (schädel von *Limnosaurus transsylvanicus* nov. gen. et spec.). Denkschriften der Kaiserlichen Akademie der Wissenschaften, Mathematisch-Naturwissenschaftliche Klasse 68:555–591.
Norman, D. B. 1980. On the ornithischian dinosaur *Iguanodon bernissartensis* from the Lower Cretaceous of Bernissart (Belgium). Mémoires de l'Institut Royal des Sciences Naturelles de Belgique 178:1–103.
Norman, D. B. 1986. On the anatomy of *Iguanodon atherfieldensis* (Ornithischia: Ornithopoda). Bulletin de l'Institut Royal des Sciences Naturelles de Belgique, Science de la Terre 56:281–372.
Norman, D. B. 1998. On Asian ornithopods (Dinosauria: Ornithischia). 3. A new species of iguanodontid dinosaur. Zoological Journal of the Linnean Society 122:291–348.
Norman, D. B. 2002. On Asian ornithopods (Dinosauria: Ornithischia). 4. *Probactrosaurus* Rozhdestvensky, 1966. Zoological Journal of the Linnean Society 136:113–144.
Norman, D. B. 2004. Basal Iguanodontia; pp. 413–437 in D. B. Weishampel, P. Dodson, and H. Osmólska (eds.), The Dinosauria: Second Edition. University of California Press, Berkeley, California.
Norman, D. B., and H.-D. Sues. 2000. Ornithopods from Kazakhstan, Mongolia and Siberia; pp. 462–479 in M. J. Benton, M. A. Shishkin, D. M. Unwin, and E. N. Kurochkin (eds.), The Age of Dinosaurs in Russia and Mongolia. Cambridge University Press, Cambridge.
Owen, R. 1842. Report on British fossil reptiles. Part II. Report of the Eleventh Meeting of the British Association for the Advancement of Science, held at Plymouth, July 1841:60–204.
Pardo-Pérez, J., B. P. Kear, M. Gómez, M. Moroni, and E. E. Maxwell. 2018. Ichthyosaurian palaeopathology: evidence of injury and disease in fossil 'fish-lizards'. Journal of Zoology 304:21–33.
Parks, W. A. 1923. *Corythosaurus intermedius*, a new species of trachodont dinosaur. University of Toronto Studies, Geological Series 15:1–57.
Paul, G. S. 2008. A revised taxonomy of the iguanodontid genera and species. Cretaceous Research 29:192–216.
Poropat, S. F. 2013. Carl Wiman's sauropods: The Uppsala Museum of Evolution's collection. GFF 135:104–119.
Poropat, S. F., and B. P. Kear. 2013a. Photographic atlas and three-dimensional reconstruction of the holotype skull of *Euhelopus zdanskyi* with description of additional cranial elements. PLoS One 8:e79932.
Poropat, S. F., and B. P. Kear. 2013b. Reassessment of coelurosaurian (Dinosauria, Theropoda) remains from the Upper Cretaceous Wangshi Group of Shandong Province, China. Cretaceous Research 45:103–113.
Prieto-Márquez, A., D. B. Weishampel, and J. R. Horner. 2006. The dinosaur *Hadrosaurus foulkii*, from the Campanian of the East Coast of North America, with a reevaluation of the genus. Acta Palaeontologica Polonica 51:77-98.
Prieto-Marquez, A. 2007. Postcranial osteology of the hadrosaurid dinosaur *Brachylophosaurus canadensis* from the Late Cretaceous of Montana; pp. 91–115 in K. Carpenter (ed.), Horns and Beaks: Ceratopsian and Ornithopod Dinosaurs. Indiana University Press, Bloomington, Indiana.
Prieto-Marquez, A. 2008. Phylogeny and historical biogeography of hadrosaurid dinosaurs, PhD dissertation, Florida State University, Tallahassee, FL, lxxv + 859 pp.
Prieto-Márquez, A. 2010a. Global phylogeny of Hadrosauridae (Dinosauria: Ornithopoda) using parsimony and Bayesian methods. Zoological Journal of the Linnean Society 159:435–502.
Prieto-Márquez, A. 2010b. The braincase and skull roof of *Gryposaurus notabilis* (Dinosauria, Hadrosauridae), with a taxonomic revision of the genus. Journal of Vertebrate Paleontology 30:838–854.

Prieto-Márquez, A. 2011a. Cranial and appendicular ontogeny of *Bactrosaurus johnsoni*, a hadrosauroid dinosaur from the Late Cretaceous of northern China. Palaeontology 54:773–792.
Prieto-Márquez, A. 2011b. A reapprisal of *Barsboldia sicinskii* (Dinosauria: Hadrosauridae) from the Late Cretaceous of Mongolia. Journal of Paleontology 85:468–477.
Prieto-Márquez, A. 2011c. Revised diagnoses of *Hadrosaurus foulkii* Leidy, 1858 (the type genus and species of Hadrosauridae Cope, 1869) and *Claosaurus agilis* Marsh, 1872 (Dinosauria: Ornithopoda) from the Late Cretaceous of North America. Zootaxa 2765:61–68.
Prieto-Márquez, A. 2014. A juvenile *Edmontosaurus* from the late Maastrichtian (Cretaceous) of North America: implications for ontogeny and phylogenetic inference in saurolophine dinosaurs. Cretaceous Research 50:282–303.
Prieto-Márquez, A., L. M. Chiappe, and S. H. Joshi. 2012. The lambeosaurine dinosaur *Magnapaulia laticaudus* from the Late Cretaceous of Baja California, northwestern Mexico. PLoS One 7: e38207.
Prieto-Márquez, A., and M. F. Guenther. 2018. Perinatal specimens of *Maiasaura* from the Upper Cretaceous of Montana (USA): insights into the early ontogeny of saurolophine hadrosaurid dinosaurs. PeerJ 6:e4734.
Prieto-Márquez, A., and S. H. Joshi. 2015. Morphological variation of pelvic skeletal elements of hadrosaurid dinosaurs quantified using Riemannian analysis of elastic curves; pp. 138–153 in P. E. Lestrel (ed.), Biological Shape Analysis. World Scientific Publishing Company, Singapore.
Prieto-Márquez, A., and M. A. Norell. 2010. Anatomy and relationships of *Gilmoreosaurus mongoliensis* (Dinosauria: Hadrosauroidea) from the Late Cretaceous of Central Asia. American Museum Novitates 3694:1–49.
Prieto-Márquez, A. and G.C. Salinas 2010. A re-evaluation of *Secernosaurus koerneri* and *Kritosaurus australis* (Dinosauria, Hadrosauridae) from the Late Cretaceous of Argentina. Journal of Vertebrate Paleontology 30(3):813–837.
Prieto-Márquez, A., and J. R. Wagner. 2009. *Pararhabdodon isonensis* and *Tsintaosaurus spinorhinus*: a new clade of lambeosaurine hadrosaurids from Eurasia. Cretaceous Research 30:1238–1246.
Prieto-Márquez, A., and J. R. Wagner. 2013. The 'unicorn' dinosaur that wasn't: a new reconstruction of the crest of *Tsintaosaurus* and the early evolution of the lambeosaurine crest and rostrum. PLoS ONE 8:e82268.
Ramírez-Velasco, A. A., M. Benammi, A. Prieto-Márquez, J. A. Ortega, and R. Hernández-Rivera. 2012. *Huehuecanauhtlus tiquichensis*, a new hadrosauroid dinosaur (Ornithischia: Ornithopoda) from the Santonian (Late Cretaceous) of Michoacán, Mexico. Canadian Journal of Earth Sciences 49:379–395.
Riabinin, A. N. 1925. [A mounted skeleton of the gigantic reptile *Trachodon amurense* nov. sp.] Izvest. Geol. Komissaya 44:1–12. [Russian with English summary].
Riabinin, A. N. 1930. [*Mandschurosaurus amurensis* nov gen., nov. sp., a hadrosaurian dinosaur from the Upper Cretaceous of Amur River]. Mémoires de la Société Paléontologique de Russie 2:1–36. [Russian]
Riabinin, A. N. 1939. [The Upper Cretaceous vertebrate fauna of south Kazakhstan]. Trudy Tsentral. Nauchno-issled. Geol. Inst 118:1–40. [Russian]
Rivera-Sylva, H. E., E. Frey, and J. R. Guzmán-Gutiérrez. 2009. Evidence of predation on the vertebra of a hadrosaurid dinosaur from the Upper Cretaceous (Campanian) of Coahuila, Mexico. Carnets de Géologie 2009:1–6.
Rozhdestvensky, A. K. 1964. [Family Hadrosauridae]; pp. 559–572 in Y. A. Orlov (ed.), Osnovyi Paleontologii. Izdatelstvo Nauka, Moscow. [Russian]
Rozhdestvensky, A. K. 1966. [New iguanodonts from Central Asia. Phylogenetic and taxonomic interrelationships of late Iguanodontidae and early Hadrosauridae]. Palaeontolgicheskii Zhurnal 3:103–116. [Russian]
Rozhdestvensky, A. K. (as Rozhdestvenskiy A. K.). 1967. New iguanodonts from Central Asia. International Geology Review 9:556–566.
Rozhdestvensky, A. K. 1968. [Hadrosaurs of Kazakhstan]; pp. 97–141 in L. P. Tatarinov, P. K. Chudinov, and M. A. Shishkin (eds.), [Upper Paleozoic and Mesozoic Amphibians and Reptiles]. Akademia Nauk S.S.S.R., Moscow. [Russian]
Rozhdestvensky, A. K. 1974. A history of dinosaur faunas from Asia and other continents and some problems of paleogeography. Trudy Sovmestnaya Sovetsko-Mongol'skaya Paleontologicheskaya Ekspiditsiya 1:107–131.
Rozhdestvensky, A. K. 1977. The study of dinosaurs in Asia. Journal of the Palaeontological Society of India 20:102–119.
Seeley, H. G. 1887. On the classification of the fossil animals commonly named Dinosauria. Proceedings of the Royal Society of London 43:165–171.
Sues, H.-D., and A. Averianov. 2009. A new basal hadrosauroid dinosaur from the Late Cretaceous of Uzbekistan and the early radiation of duck-billed dinosaurs. Proceedings of the Royal Society B 276:2549–2555.
Taquet, P. 1976. Géologie et paléontologie du gisement de Gadoufaoua (Aptien du Niger). 191 pp. Cahiers de paleontologie, Éditions du Centre National de la Recherche Scientifique, Paris. [English abstract]
Taquet, P. 1991. The status of *Tsintaosaurus spinorhinus* Young, 1958 (Dinosauria); pp. 63–64 in Z. Kielan-Jaworowska, N. Heintz, and H. A. Nakrem (eds.), Fifth Symposium on Mesozoic Terrestrial Ecosystems and Biota, Extended Abstracts: Contributions from the Paleontological Museum. University of Oslo.
Tsogtbaatar K., D. B. Weishampel, D. C. Evans, and M. Watabe. 2019. A new hadrosauroid (Dinosauria: Ornithopoda) from the latest Cretaceous Baynshire Formation of the Gobi Desert (Mongolia). PLoS ONE 14:e0208480.
Verdú, F. J., P. Godefroit, R. Royo-Torres, A. Cobos, and L. Alcalá. 2017. Individual variation in the postcranial skeleton of the Early Cretaceous *Iguanodon bernissartensis* (Dinosauria: Ornithopoda). Cretaceous Research 74:65–86.
Verdú, F. J., R. Royo-Torres, A. Cobos, and L. Alcalá. 2015. Perinates of a new species of *Iguanodon* (Ornithischia: Ornithopoda) from the lower Barremian of Galve (Teruel, Spain). Cretaceous Research 56:250–264.
Wang, R.-F., H.-L. You, S.-Z. Wang, S.-C. Xu, J. Yi, L.-J. Xie, L. Jia, and H. Xing. 2017. A second hadrosauroid dinosaur from the early Late Cretaceous of Zuoyun, Shanxi Province, China. Historical Biology 29:17–24.
Wang, R.-F., H.-L. You, S.-C. Xu, S.-Z. Wang, J. Yi, L.-J. Xie, L. Jia, and Y.-X. Li. 2013. A new hadrosauroid dinosaur from the early Late Cretaceous of Shanxi Province, China. PLoS ONE 8:e77058.
Wang, X., R. Pan, R. J. Butler, and P. M. Barrett. 2011. The postcranial skeleton of the iguanodontian ornithopod *Jinzhousaurus yangi* from the Lower Cretaceous Yixian Formation of western Liaoning, China. Earth and Environmental Science Transactions of the Royal Society of Edinburgh 101:135–159.
Wang, X., and X. Xu. 2001. A new iguanodontid (*Jinzhousaurus yangi* gen. et sp. nov.) from the Yixian Formation of western Liaoning, China. Chinese Science Bulletin 46:1669–1672.
Weishampel, D. B., and J. R. Horner. 1986. The hadrosaurid dinosaurs from the Iren Dabasu fauna (People's Republic of China, Late Cretaceous). Journal of Vertebrate Paleontology 6:38–45.
Weishampel, D. B., and J. R. Horner. 1990. Hadrosauridae; pp. 534–561 in D. B. Weishampel, P. Dodson, and H. Osmólska (eds.), The Dinosauria. University of California Press, Berkeley.
Weishampel, D. B., D. B. Norman, and D. Grigorescu. 1993. *Telmatosaurus transsylvanicus* from the Late Cretaceous of Romania: the most basal hadrosaurid dinosaur. Palaeontology 36:361–385.
Wilson, J. A., and P. Upchurch. 2009. Redescription and reassessment of *Euhelopus zdanskyi* (Dinosauria: Sauropoda) from the Early Cretaceous of China. Journal of Systematic Palaeontology 7:199–239.
Wiman, C. 1929. Die Kreide-Dinosaurier aus Shantung. Palaeontologia Sinica (Series C) 6:1–67.
Wu, W.-H., P. Godefroit, and D.-Y. Hu. 2010. *Bolong yixianensis* gen. et sp. nov.: a new iguanodontoid dinosaur from the Yixian Formation of western Liaoning, China. Geology and Resources 19:127–133.
Xing, H., D. Wang, F. Han, C. Sullivan, Q. Ma, Y. He, D. W. E. Hone, R. Yan, F. Du, and X. Xu. 2014a. A new basal hadrosauroid dinosaur (Dinosauria: Ornithopoda) with transitional features from the Late Cretaceous of Henan Province, China. PLoS ONE 9:e98821.

Xing, H., X. Zhao, K. Wang, D. Li, S. Chen, J. C. Mallon, Y. Zhang, and X. Xu. 2014b. Comparative osteology and phylogenetic relationship of *Edmontosaurus* and *Shantungosaurus* (Dinosauria: Hadrosauridae) from the Upper Cretaceous of North America and East Asia. Acta Geologica Sinica 88:1623–1652.

Xing, H., J. C. Mallon, and M. L. Currie. 2017. Supplementary cranial description of the types of *Edmontosaurus regalis* (Ornithischia: Hadrosauridae), with comments on the phylogenetics and biogeography of Hadrosaurinae. PLoS ONE 12: e0175253.

Xu, X., X.-J. Zhao, J.-C. Lü, W.-B. Huang, Z.-Y. Li, and Z.-M. Dong. 2000. A new iguanodontian from Sangping Formation of Neixiang, Henan and its stratigraphical implication. Vertebrata PalAsiatica 38:176–191. [in Chinese with English summary].

Yan, J., Chen, J. F., Xie, Z., Gao, T. S., Foland, K. A., Zhang, X. D., and Liu, M. W. 2005. [Studies on petrology and geochemistry of the Late Cretaceous basalts and mantlederived xenoliths from eastern Shandong]. Acta Petrologica Sinica 21:99–112. [Chinese with English abstract].

Young, C.-C. 1958. The dinosaurian remains of Laiyang, Shantung. Palaeontologia Sinica (Series C) 16:1–138.

Zhang, J.-L., Q. Wang, S.-X. Jiang, X. Cheng, N. Li, R. Qiu, X.-J. Zhang, and X.-L. Wang. 2017. Review of historical and current research on the Late Cretaceous dinosaurs and dinosaur eggs from Laiyang, Shandong. Vertebrata PalAsiatica 55:187–200.

Zhang, Y.-G., K.-B. Wang, S.-Q. Chen, D. Liu, and H. Xing. 2020. Osteological re-assessment and taxonomic revision of "*Tanius laiyangensis*" (Ornithischia: Hadrosauroidea) from the Upper Cretaceous of Shandong, China. Anatomical Record 303:790–800.

Zhen, S. 1976. A new species of hadrosaur from Shandong. Vertebrata PalAsiatica 14:166–168. [Chinese with English abstract]

Zheng, R., A. A. Farke, and G.-S. Kim. 2011. A photographic atlas of the pes from a hadrosaurine hadrosaurid dinosaur. PalArch's Journal of Vertebrate Palaeontology 8:1–12.

Submitted August 7, 2020; revisions received November 20, 2020; accepted November 29, 2020.
Handling Editor: Lindsay Zanno.